

# Exponentially Stable Observer-based Controller for VTOL-UAVs without Velocity Measurements

Hashim A. Hashim

**Abstract**—There is a great demand for vision-based robotics solutions that can operate using Global Positioning Systems (GPS), but are also robust against GPS signal loss and gyroscope failure. This paper investigates the estimation and tracking control in application to a Vertical Take-Off and Landing (VTOL) Unmanned Aerial Vehicle (UAV) in six degrees of freedom (6 DoF). A full state observer for the estimation of VTOL-UAV motion parameters (attitude, angular velocity, position, and linear velocity) is proposed on the Lie Group of  $\mathbb{SE}_2(3) \times \mathbb{R}^3 = \mathbb{SO}(3) \times \mathbb{R}^9$  with almost globally exponentially stable closed loop error signals. Thereafter, a full state observer-based controller for the VTOL-UAV motion parameters is proposed on the Lie Group with a guaranteed almost global exponential stability. The proposed approach produces good results without the need for angular and linear velocity measurements (without a gyroscope and GPS signals) utilizing only a set of known landmarks obtained by a vision-aided unit (monocular or stereo camera). The equivalent quaternion representation on  $\mathbb{S}^3 \times \mathbb{R}^9$  is provided in the Appendix. The observer-based controller is presented in a continuous form while its discrete version is tested using a VTOL-UAV simulation that incorporates large initial error and uncertain measurements. The proposed observer is additionally tested experimentally on a real-world UAV flight dataset.

**Index Terms**—Unmanned aerial vehicle, nonlinear filter algorithm, autonomous navigation, tracking control, feature measurement, observer-based controller, localization, asymptotic stability.

## I. INTRODUCTION

**S**UCCESSFUL inertial navigation of Unmanned Aerial Vehicles (UAVs), underwater vehicles, and ground vehicles, among other engineering applications, requires robust solutions for attitude (orientation), angular velocity, position, and linear velocity estimation and tracking control. It has long been recognized that rigid-body motion parameters cannot be obtained directly, but are instead reconstructed from sensor measurements. Rigid-body's attitude can be reconstructed algebraically using inertial-frame observations and corresponding body-frame measurements [1], [2] followed by position reconstruction. However, better attitude and pose estimation solutions are offered by Kalman filters [3]–[5], nonlinear filters on the *Special Orthogonal Group*  $\mathbb{SO}(3)$  that mimic the true attitude dynamics geometry [6], [7], and nonlinear filters on the *Special Euclidean Group*  $\mathbb{SE}(3)$  that mimic the true pose (attitude + position) dynamics geometry [8], [9]. The true attitude dynamics representation relies on angular velocity typically measured by a gyroscope. The true pose, on the

other hand, requires measurements of both angular and linear velocity where the linear velocity is generally made available by the Global Positioning System (GPS) sensors [8]–[14]. Hence, obtaining linear velocity in a GPS-denied region poses a challenge [10], [15]–[17]. Thereby, the filters in [3], [4], [6]–[9] are not suitable for pose estimation when a gyroscope fails and/or a reliable GPS signal is not available. Consequently, multiple GPS-independent navigation solutions that rely solely on angular velocity, landmark, and inertial measurements have been proposed for the estimation of attitude, position, and linear velocity of a vehicle, such as adaptive Kalman filter [18], extended Kalman filter [11], invariant extended Kalman filter on the Lie Group of Extended Special Euclidean Group  $\mathbb{SE}_2$  [19], and nonlinear stochastic filters on  $\mathbb{SE}_2$  [10], [17]. However, none of the above solutions account for gyroscope failure, immediate replacement of which may prove challenging and expensive [20]. As such, full observers that bypass measuring angular and linear velocity, and provide accurate estimates of attitude, angular velocity, position, and linear velocity are still lacking.

On the other hand, control of UAVs, in particular quadrotors and Vertical Take-Off and Landing (VTOL)-UAVs, has drawn attention of the control community in the recent years. Proposed solutions include backstepping control [21], cascaded control [22], sliding mode control [23], [24], a hierarchical design procedure for the position control [25], [26], and others. The design of the above-mentioned controllers implies the ready availability of accurate attitude, position, and angular velocity which can be enabled only by high accuracy and precision expensive sensors. Owing to large size, expensive sensors are unsuitable for low-cost small-sized UAVs [8]. Low-cost UAVs are commonly equipped with low-cost sensors, such as an Inertial Measurement Unit (IMU) and a vision unit (monocular or stereo camera) [10]. Note that a low-cost IMU provides noisy angular velocity measurements [7]. Therefore, integrating the above controllers with low-cost vision and IMU units may lead to undesirable results [10]. Alternatively, the vehicle's orientation, position, and angular velocity can be obtained by a combination of an Image-Based Visual Servoing (IBVS) algorithm and an IMU. For instance, trajectory of a VTOL-UAV can be controlled based on the information supplied by IBVS and an IMU [27]–[30]. The aforementioned control architecture incorporates two loops, where the inner loop controls the vehicle's orientation and angular velocity employing IMU measurements, while the outer loop controls the position using the thrust calculated based on the vision measurements. Nevertheless, the state vector of most proposed IBVS solutions relies on Euler angles which are subject to singularity, and therefore fail to represent the attitude at certain

This work was supported in part by National Sciences and Engineering Research Council of Canada (NSERC), under the grants RGPIN-2022-04937 and DGEER-2022-00103.

H. A. Hashim is with the Department of Mechanical and Aerospace Engineering, Carleton University, Ottawa, Ontario, K1S-5B6, Canada, email: hhashim@carleton.ca

configurations [31], [32]. Furthermore, the solutions reported in [27]–[30] are only locally stable. Considering the high nonlinearity of the true motion dynamics of a VTOL-UAV, this paper proposes an observer-based controller on the Lie Group that represents vehicle's orientation on  $\mathbb{SO}(3)$  providing a unique, global, and nonsingular representation of the VTOL-UAV motion.

*Contributions:* Motivated by the shortcomings of the existing literature solutions and the high demand for observer-based controllers, the contributions of this work are as follows:

- (1) A nonlinear observer for attitude, angular velocity, position, and linear velocity that mimics the true motion dynamics of a VTOL-UAV is proposed on the Lie Group of  $\mathbb{SE}_2(3) \times \mathbb{R}^3$ .
- (2) The proposed observer operates based on measurements obtained from a vision unit without the need for angular and linear velocity measurements.
- (3) The closed loop error signals of the observer are shown to be almost globally exponentially stable.
- (4) A novel control law posed on the Lie Group is proposed. In combination with the proposed observer it forms an observer-based controller whose closed loop error signals are almost globally exponentially stable.
- (5) The proposed approach is continuous, and its discrete version is tested at a low sampling rate through simulation and experimentally.

The proposed observer-based controller allows for successful mission completion even in case of gyroscope failure. In addition, it is suitable for both GPS and GPS-denied applications. To the best of our knowledge, this work is the first to present an observer-based controller on the Lie Group that mimics the true VTOL-UAV motion dynamics and accurately estimates attitude, angular velocity, position, and linear velocity.

*Structure:* The rest of the paper is organized as follows: Section II presents preliminaries; Section III formulates the problem; Section IV proposes a novel nonlinear observer for a VTOL-UAV; Section V presents a VTOL-UAV control strategy; Section VI summarizes the discrete implementation steps; The robustness of the proposed approach is validated in Section VII through simulation and experimental results; Finally, Section VIII contains concluding remarks.

Table I provides some important notation that will be used throughout the paper.

## II. PRELIMINARIES

The set of real numbers, an  $n$ -by- $m$  real dimensional space, and non-negative real numbers are represented by  $\mathbb{R}$ ,  $\mathbb{R}^{n \times m}$ , and  $\mathbb{R}_+$ , respectively.  $\|x\| = \sqrt{x^\top x}$  refers to an Euclidean norm of a vector  $x \in \mathbb{R}^n$ , while  $\|M\|_F = \sqrt{\text{Tr}\{MM^*\}}$  denotes the Frobenius norm of a matrix  $M \in \mathbb{R}^{n \times m}$  where  $*$  is the conjugate transpose. The set of eigenvalues of a given matrix  $M \in \mathbb{R}^{n \times n}$  is represented by  $\lambda(M) = \{\lambda_1, \lambda_2, \dots, \lambda_n\}$  with  $\bar{\lambda}_M = \bar{\lambda}(M)$  and  $\underline{\lambda}_M = \underline{\lambda}(M)$  being the set's maximum and minimum values, respectively.  $0_{n \times m}$  represents an  $n$ -by- $m$  dimensional zero matrix, while  $\mathbf{I}_n$  is an  $n$ -by- $n$  identity matrix. Consider a vehicle navigating in 3D space with

- $\{\mathcal{B}\} \triangleq \{e_{B1}, e_{B2}, e_{B3}\}$  signifying the fixed body-frame attached to a vehicle and

TABLE I  
NOMENCLATURE

$\{\mathcal{B}\} / \{\mathcal{I}\}$	:	fixed body-frame / fixed inertial-frame
$\mathbb{SO}(3)$	:	Special Orthogonal Group of order 3
$\mathfrak{so}(3)$	:	Lie-algebra of $\mathbb{SO}(3)$
$\mathbb{SE}(3)$	:	Special Euclidean Group, $\mathbb{SE}(3) = \mathbb{SO}(3) \times \mathbb{R}^3$
$\mathbb{SE}_2(3)$	:	Extended $\mathbb{SE}(3)$ , $\mathbb{SE}_2(3) = \mathbb{SE}(3) \times \mathbb{R}^3$
$\mathbb{S}^3$	:	Three-unit-sphere
$\mathbb{R}^{n \times m}$	:	$n$ -by- $m$ real dimensional space
$R, \hat{R}$ , and $R_d$	:	<b>True (unknown)</b> , estimated, and desired attitude, $R, \hat{R}, R_d \in \mathbb{SO}(3)$
$\Omega, \hat{\Omega}$ , and $\Omega_d$	:	<b>True (unknown)</b> , estimated, and desired angular velocity, $\Omega, \hat{\Omega}, \Omega_d \in \mathbb{R}^3$
$P, \hat{P}$ , and $P_d$	:	<b>True (unknown)</b> , estimated, and desired position, $P, \hat{P}, P_d \in \mathbb{R}^3$
$V, \hat{V}$ , and $V_d$	:	<b>True (unknown)</b> , estimated, and desired linear velocity, $V, \hat{V}, V_d \in \mathbb{R}^3$
$X$ and $\hat{X}$	:	<b>True (unknown)</b> and estimated navigation, $X, \hat{X} \in \mathbb{SE}_2(3)$
$\mathcal{T} \in \mathbb{R}^3$	:	Rotational torque input
$\mathfrak{S} \in \mathbb{R}$	:	Thrust magnitude input
$y_i^{\mathcal{B}} \in \mathbb{R}^3$	:	The $i$ th body-frame vector measurement
$v_i^{\mathcal{I}} \in \mathbb{R}^3$	:	The $i$ th inertial-frame observation
$z_j^{\mathcal{B}} \in \mathbb{R}^3$	:	Measured $j$ th landmark at body-frame
$p_j^{\mathcal{I}} \in \mathbb{R}^3$	:	The $j$ th landmark observation at inertial-frame
$b_{\star}^{\mathcal{B}} \in \mathbb{R}^3$	:	The $\star$ th bias component of $y_{\star}^{\mathcal{B}}$ measurement
$n_{\star}^{\mathcal{B}} \in \mathbb{R}^3$	:	The $\star$ th noise component of $y_{\star}^{\mathcal{B}}$ measurement
$R_y \in \mathbb{SO}(3)$	:	Reconstructed attitude
$\tilde{R}_o \in \mathbb{SO}(3)$	:	Attitude estimation error
$\tilde{\Omega}_o \in \mathbb{R}^3$	:	Angular velocity estimation error
$\tilde{P}_o \in \mathbb{R}^3$	:	Position estimation error
$\tilde{V}_o \in \mathbb{R}^3$	:	Linear velocity estimation error
$\tilde{R}_c \in \mathbb{SO}(3)$	:	Attitude control error
$\tilde{\Omega}_c \in \mathbb{R}^3$	:	Angular velocity control error
$\tilde{P}_c \in \mathbb{R}^3$	:	Position control error
$\tilde{V}_c \in \mathbb{R}^3$	:	Linear velocity control error
$F \in \mathbb{R}^3$	:	Intermediary control input
$m$ and $J$	:	Mass and inertia of the UAV, $m \in \mathbb{R}$ and $J \in \mathbb{R}^{3 \times 3}$
$Q, \hat{Q}$ , and $Q_d$	:	True (unknown), estimated, and desired unit-quaternion vector, $Q, \hat{Q}, Q_d \in \mathbb{S}^3$
$\mathcal{R}_Q \in \mathbb{SO}(3)$	:	Attitude representation obtained using unit-quaternion vector

- $\{\mathcal{I}\} \triangleq \{e_1, e_2, e_3\}$  representing the fixed inertial-frame. The standard basis vectors of  $\mathbb{R}^3$  are denoted by  $e_1 := [1, 0, 0]^\top$ ,  $e_2 := [0, 1, 0]^\top$ , and  $e_3 := [0, 0, 1]^\top$ . Note that for  $x \in \mathbb{R}^n$  the  $m$ th derivative of  $x$  is defined by  $x^{(m)} = dx^m/dt^m$ .

### A. Lie Group of $\mathbb{SO}(3)$ and Properties

The vehicle's orientation in 3D space is termed attitude commonly represented as a rotation matrix in  $\{\mathcal{B}\}$  defined by  $R \in \mathbb{SO}(3) \subset \mathbb{R}^{3 \times 3}$ . The notation  $\mathbb{SO}(3)$  refers to the 3-dimensional *Special Orthogonal Group* defined by

$$\mathbb{SO}(3) = \{R \in \mathbb{R}^{3 \times 3} \mid RR^\top = R^\top R = \mathbf{I}_3, \det(R) = +1\}$$

Define  $T_R\mathbb{SO}(3) \in \mathbb{R}^{3 \times 3}$  as a tangent space of  $\mathbb{SO}(3)$  at point  $R \in \mathbb{SO}(3)$ . The *Lie-algebra* of  $\mathbb{SO}(3)$  is termed  $\mathfrak{so}(3)$  and follows the map  $[\cdot]_{\times} : \mathbb{R}^3 \rightarrow \mathfrak{so}(3)$

$$\mathfrak{so}(3) = \left\{ [y]_{\times} \in \mathbb{R}^{3 \times 3} \mid [y]_{\times}^{\top} = -[y]_{\times} \right\}$$

$$[y]_{\times} = \begin{bmatrix} 0 & -y_3 & y_2 \\ y_3 & 0 & -y_1 \\ -y_2 & y_1 & 0 \end{bmatrix} \in \mathfrak{so}(3), \quad y = \begin{bmatrix} y_1 \\ y_2 \\ y_3 \end{bmatrix}$$

with  $[y]_{\times}$  being a skew symmetric matrix such that  $[y]_{\times} z = y \times z$  for all  $y, z \in \mathbb{R}^3$ . The inverse mapping of  $[\cdot]_{\times}$  to  $\mathbb{R}^3$  is defined by  $\mathbf{vex} : \mathfrak{so}(3) \rightarrow \mathbb{R}^3$  such that

$$\mathbf{vex}([y]_{\times}) = y, \quad \forall y \in \mathbb{R}^3 \quad (1)$$

The anti-symmetric projection operator  $\mathcal{P}_a$  on the  $\mathfrak{so}(3)$  is defined by

$$\mathcal{P}_a(A) = \frac{1}{2}(A - A^{\top}) \in \mathfrak{so}(3), \quad \forall A \in \mathbb{R}^{3 \times 3} \quad (2)$$

$$\mathbf{vex}(\mathcal{P}_a(A)) = \frac{1}{2}[A_{32} - A_{23}, A_{13} - A_{31}, A_{21} - A_{12}]^{\top} \quad (3)$$

where  $A := [A_{ij}]_{i,j=1,2,3}$ . Define  $\|R\|_{\text{I}}$  as the normalized Euclidean distance of  $R \in \mathbb{SO}(3)$  such that

$$\|R\|_{\text{I}} = \frac{1}{4} \text{Tr}\{\mathbf{I}_3 - R\} \in [0, 1] \quad (4)$$

It is worth noting that  $-1 \leq \text{Tr}\{R\} \leq 3$  and  $\|R\|_{\text{I}} = \frac{1}{8}\|\mathbf{I}_3 - R\|_{\text{F}}^2$  [32]. Visit [7], [32] for more information.

### B. $\mathbb{SE}(3)$ , $\mathbb{SE}_2(3)$ , and Tangent Space

Let the vehicle's orientation, position, and linear velocity be denoted as  $R \in \mathbb{SO}(3)$ ,  $P \in \mathbb{R}^3$ , and  $V \in \mathbb{R}^3$ , respectively. The *Special Euclidean Group* is defined by  $\mathbb{SE}(3) := \mathbb{SO}(3) \times \mathbb{R}^3 \subset \mathbb{R}^{4 \times 4}$  where  $T \in \mathbb{SE}(3)$  is a homogeneous transformation matrix defined as follows:

$$T = \begin{bmatrix} R^{\top} & P \\ 0_{1 \times 3} & 1 \end{bmatrix}, \quad T^{-1} = \begin{bmatrix} R & -RP \\ 0_{1 \times 3} & 1 \end{bmatrix} \quad (5)$$

visit [8] for more information.  $\mathbb{SE}_2(3)$  is the extended form of the *Special Euclidean Group* introduced by [19] where  $\mathbb{SE}_2(3) = \mathbb{SO}(3) \times \mathbb{R}^3 \times \mathbb{R}^3 \subset \mathbb{R}^{5 \times 5}$  such that

$$\mathbb{SE}_2(3) = \{X \in \mathbb{R}^{5 \times 5} \mid R \in \mathbb{SO}(3), P, V \in \mathbb{R}^3\} \quad (6)$$

with  $R$ ,  $P$ , and  $V$  being vehicle's attitude, position and linear velocity, respectively, and

$$X = \mathcal{N}(R^{\top}, P, V) = \begin{bmatrix} R^{\top} & P & V \\ 0_{1 \times 3} & 1 & 0 \\ 0_{1 \times 3} & 0 & 1 \end{bmatrix} \in \mathbb{SE}_2(3) \quad (7)$$

being its homogeneous navigation matrix (for more details see [10], [17]). Note that

$$X^{-1} = \begin{bmatrix} R & -RP & -RV \\ 0_{1 \times 3} & 1 & 0 \\ 0_{1 \times 3} & 0 & 1 \end{bmatrix} \in \mathbb{SE}_2(3)$$

The tangent space of  $\mathbb{SE}_2(3)$  at point  $X \in \mathbb{SE}_2(3)$  is defined by  $T_X\mathbb{SE}_2(3) \in \mathbb{R}^{5 \times 5}$ . Define the submanifold  $\mathcal{U}_{\mathcal{M}} = \mathfrak{so}(3) \times \mathbb{R}^3 \times \mathbb{R}^3 \times \mathbb{R} \subset \mathbb{R}^{5 \times 5}$  as

$$\mathcal{U}_{\mathcal{M}} = \{u([\Omega]_{\times}, V, a, \kappa) \mid [\Omega]_{\times} \in \mathfrak{so}(3), V, a \in \mathbb{R}^3, \kappa \in \mathbb{R}\}$$

$$U = u([\Omega]_{\times}, V, a, \kappa) = \begin{bmatrix} [\Omega]_{\times} & V & a \\ 0_{1 \times 3} & 0 & 0 \\ 0_{1 \times 3} & \kappa & 0 \end{bmatrix} \in \mathcal{U}_{\mathcal{M}} \quad (8)$$

### C. Unit-quaternion

Let us define a set of 3-unit-sphere

$$\mathbb{S}^3 = \{Q = [q_0, q^{\top}]^{\top} \in \mathbb{R}^4 \mid \|Q\| = \sqrt{q_0^2 + q^{\top}q} = 1\}$$

where  $q_0 \in \mathbb{R}$  and  $q \in \mathbb{R}^3$ . Consider the inverse of  $Q \in \mathbb{S}^3$  to be  $Q^{-1} = [q_0 \quad -q^{\top}]^{\top} \in \mathbb{S}^3$ . Let  $\odot$  be a quaternion product. For  $Q_1 = [q_{01} \quad q_1^{\top}]^{\top} \in \mathbb{S}^3$  and  $Q_2 = [q_{02} \quad q_2^{\top}]^{\top} \in \mathbb{S}^3$ , one has

$$Q_1 \odot Q_2 = \begin{bmatrix} q_{01}q_{02} - q_1^{\top}q_2 \\ q_{01}q_2 + q_{02}q_1 + [q_1]_{\times}q_2 \end{bmatrix}$$

The mapping from  $\mathbb{S}^3$  to  $\mathbb{SO}(3)$  is given by

$$\mathcal{R}_Q = (q_0^2 - \|q\|^2)\mathbf{I}_3 + 2qq^{\top} - 2q_0[q]_{\times} \in \mathbb{SO}(3) \quad (9)$$

The following two identities will be utilized in the subsequent derivations:

$$[Ry]_{\times} = R[y]_{\times}R^{\top}, \quad y \in \mathbb{R}^3, R \in \mathbb{SO}(3) \quad (10)$$

$$\text{Tr}\{A[y]_{\times}\} = \text{Tr}\{\mathcal{P}_a(A)[y]_{\times}\}, \quad y \in \mathbb{R}^3, A \in \mathbb{R}^{3 \times 3}$$

$$= -2\mathbf{vex}(\mathcal{P}_a(A))^{\top}y \quad (11)$$

## III. PROBLEM FORMULATION AND MEASUREMENTS

Consider a UAV navigating in 3D space. Let its true attitude, angular velocity, position, and linear velocity be unknown and described by  $R \in \mathbb{SO}(3)$ ,  $\Omega \in \mathbb{R}^3$ ,  $P \in \mathbb{R}^3$ , and  $V \in \mathbb{R}^3$ , respectively. Note that while  $R, \Omega \in \{\mathcal{B}\}$  are defined with respect to the body-frame,  $P, V \in \{\mathcal{I}\}$  are represented with respect to the inertial-frame. The dynamical equations of a VTOL-UAV are given by

$$\text{Rotation} \begin{cases} \dot{R} &= -[\Omega]_{\times}R \\ J\dot{\Omega} &= [J\Omega]_{\times}\Omega + \mathcal{T} \end{cases}, \quad R, \Omega \in \{\mathcal{B}\} \quad (12)$$

$$\text{Translation} \begin{cases} \dot{P} &= V \\ \dot{V} &= ge_3 - \frac{\mathfrak{S}}{m}R^{\top}e_3 \end{cases}, \quad P, V \in \{\mathcal{I}\} \quad (13)$$

with  $\mathcal{T} \in \mathbb{R}^3$  being the external torque input,  $\mathfrak{S} \in \mathbb{R}$  being the thrust magnitude input in the direction of  $e_{B3}$  (see Fig. 1), and  $J \in \mathbb{R}^{3 \times 3}$  being a constant symmetric positive definite inertia matrix.  $e_3 = [0, 0, 1]^{\top}$ ,  $m$ , and  $g$  denote standard basis vector, vehicle's constant mass, and gravitational acceleration, respectively. Note that  $J, \mathcal{T} \in \{\mathcal{B}\}$ . The set in (12) describes the true VTOL-UAV rotational dynamics, while the set in (13) describes the true VTOL-UAV translational dynamics. It is apparent that the nonlinear attitude dynamics in (12) follow the map  $\mathbb{SO}(3) \times \mathfrak{so}(3) \rightarrow T_R\mathbb{SO}(3)$ . The nonlinear dynamics in (12) and (13) can be rewritten compactly as follows:

$$\begin{cases} \dot{X} &= XU - \mathcal{G}X \\ J\dot{\Omega} &= [J\Omega]_{\times}\Omega + \mathcal{T} \end{cases} \quad (14)$$

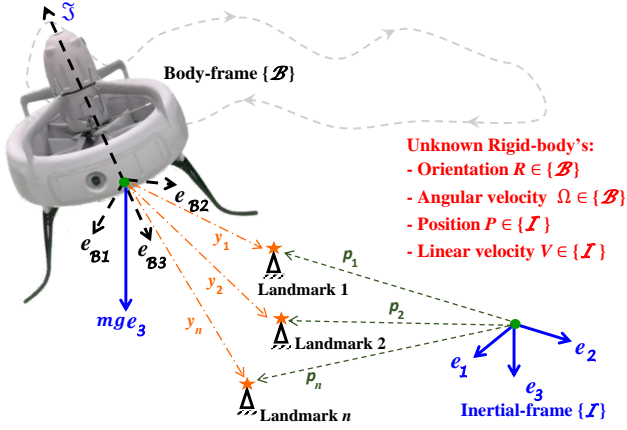


Fig. 1. VTOL-UAV estimation and tracking control problem.

where the navigation matrix  $X \in \mathbb{SE}_2(3)$  is as defined

$$\text{in (7), } U = \begin{bmatrix} [\Omega]_{\times} & 0_{3 \times 1} & -\frac{\mathfrak{g}}{m} e_3 \\ 0_{1 \times 3} & 0 & 0 \\ 0_{1 \times 3} & 1 & 0 \end{bmatrix} \in \mathcal{U}_{\mathcal{M}}, \text{ and } \mathcal{G} = \begin{bmatrix} u([\Omega]_{\times}, 0_{3 \times 1}, -\frac{\mathfrak{g}}{m} e_3, 1) \\ 0_{3 \times 3} & 0_{3 \times 1} & -g e_3 \\ 0_{1 \times 3} & 0 & 0 \\ 0_{1 \times 3} & 1 & 0 \end{bmatrix} \in \mathcal{U}_{\mathcal{M}}, \text{ see (8). The nonlinear} \\ u(0_{3 \times 3}, 0_{3 \times 1}, -g e_3, 1)$$

dynamics in (14) follow the map  $\mathbb{SE}_2(3) \times \mathcal{U}_{\mathcal{M}} \rightarrow T_X \mathbb{SE}_2(3)$  with  $\dot{X} \in T_X \mathbb{SE}_2(3)$ . Fig. 1 schematically depicts the VTOL-UAV estimation and tracking control problem.

### A. Inertial Measurements

Considering the fact that the true VTOL-UAV motion parameters  $R$ ,  $\Omega$ ,  $P$ , and  $V$  are unknown, the estimation process requires sensor measurements. For simplicity, let the superscripts  $\mathcal{I}$  and  $\mathcal{B}$  indicate association with inertial-frame and body-frame, respectively. Given a set of observations in  $\{\mathcal{I}\}$  and the corresponding  $\{\mathcal{B}\}$  measurements, the orientation of a vehicle can be obtained as follows [6], [7]:

$$y_i^{\mathcal{B}} = R v_i^{\mathcal{I}} + b_i^{\mathcal{B}} + n_i^{\mathcal{B}} \in \mathbb{R}^3 \quad (15)$$

where  $y_i^{\mathcal{B}}$  refers to vector measurements,  $v_i^{\mathcal{I}}$  refers to a known observation,  $b_i^{\mathcal{B}}$  denotes unknown constant bias, and  $n_i^{\mathcal{B}}$  describes unknown random noise associated with the  $i$ th measurement for all  $i = 1, 2, \dots, N_1$ . Note that (15) represents a typical low-cost IMU module (e.g., magnetometer and accelerometer). Moreover, attitude and position can be obtained via a vision unit (monocular or stereo camera) using a group of known landmarks in  $\{\mathcal{I}\}$  and their measurements in  $\{\mathcal{B}\}$  where the  $j$ th measurement is defined by [8]

$$z_j^{\mathcal{B}} = R(p_j^{\mathcal{I}} - P) + b_j^{\mathcal{B}} + n_j^{\mathcal{B}} \in \mathbb{R}^3 \quad (16)$$

with  $p_j^{\mathcal{I}}$  denoting a known landmark,  $b_j^{\mathcal{B}}$  denoting unknown bias (constant), and  $n_j^{\mathcal{B}}$  denoting unknown random noise for all  $j = 1, 2, \dots, N_2$ . Define  $s_j$  as the  $j$ th measurement sensor confidence level, and let  $s_c = \sum_{j=1}^{N_2} s_j$ . Define the landmark

weighted geometric center (observations and measurements) as

$$p_c = \frac{1}{s_c} \sum_{j=1}^{N_2} s_j p_j^{\mathcal{I}}, \quad z_c = \frac{1}{s_c} \sum_{j=1}^{N_2} s_j z_j^{\mathcal{B}} \quad (17)$$

The measurement in (15) can be reformulated in terms of the homogeneous transformation matrix  $T \in \mathbb{SE}(3)$  in (5) as  $\bar{y}_i^{\mathcal{B}} = T^{-1} \bar{v}_i^{\mathcal{I}} + \bar{b}_i^{\mathcal{B}} + \bar{n}_i^{\mathcal{B}} \in \mathbb{R}^4$  where  $\bar{y}_i^{\mathcal{B}} = [(y_i^{\mathcal{B}})^{\top}, 0]^{\top}$ ,  $\bar{v}_i^{\mathcal{I}} = [(v_i^{\mathcal{I}})^{\top}, 0]^{\top}$ ,  $\bar{b}_i^{\mathcal{B}} = [(b_i^{\mathcal{B}})^{\top}, 0]^{\top}$ , and  $\bar{n}_i^{\mathcal{B}} = [(n_i^{\mathcal{B}})^{\top}, 0]^{\top}$ . Likewise, the measurement in (16) can be described with respect to  $T \in \mathbb{SE}(3)$  as  $\bar{z}_j^{\mathcal{B}} = T^{-1} \bar{p}_j^{\mathcal{I}} + \bar{b}_j^{\mathcal{B}} + \bar{n}_j^{\mathcal{B}} \in \mathbb{R}^4$  where  $\bar{z}_j^{\mathcal{B}} = [(z_j^{\mathcal{B}})^{\top}, 1]^{\top}$ ,  $\bar{p}_j^{\mathcal{I}} = [(p_j^{\mathcal{I}})^{\top}, 1]^{\top}$ ,  $\bar{b}_j^{\mathcal{B}} = [(b_j^{\mathcal{B}})^{\top}, 0]^{\top}$ , and  $\bar{n}_j^{\mathcal{B}} = [(n_j^{\mathcal{B}})^{\top}, 0]^{\top}$ .

**Assumption 1.** (Pose observability) The pose of a vehicle  $T \in \mathbb{SE}(3)$  can be obtained if one of the following three conditions is met:

- A1. observations in  $\{\mathcal{I}\}$  and the associated  $\{\mathcal{B}\}$  measurements of a minimum of one landmark as in (16) and two different inertial vectors as in (15) are non-collinear.
- A2. observations in  $\{\mathcal{I}\}$  and the associated  $\{\mathcal{B}\}$  measurements of a minimum of two different landmarks as in (16) and one inertial vector as in (15) are non-collinear.
- A3. observations in  $\{\mathcal{I}\}$  and the associated  $\{\mathcal{B}\}$  measurements of a minimum of three different landmarks as in (16) are non-collinear.

It is worth mentioning that Assumption 1 is standard for pose filtering [8], [9].

**Assumption 2.** Let  $P_d$  denote the desired position of a VTOL-UAV with  $\dot{P}_d = V_d$ ,  $\ddot{P}_d$ ,  $P_d^{(3)}$ , and  $P_d^{(4)}$  being its first, second, third, and fourth derivatives, respectively. Also, let  $\Omega_d$  and  $\dot{\Omega}_d$  be the desired angular velocity and its rate of change, respectively.  $P_d$ ,  $V_d$ ,  $\ddot{P}_d$ ,  $P_d^{(3)}$ ,  $P_d^{(4)}$ ,  $\Omega_d$ , and  $\dot{\Omega}_d$  are assumed to be uniformly upper bounded in time.

**Lemma 1.** Let  $R \in \mathbb{SO}(3)$ , and consider the definitions in (3) and (4). Consequently, the following holds:

$$\|\text{vex}(\mathcal{P}_a(R))\|^2 = 4(1 - \|R\|_{\mathbb{I}}) \|R\|_{\mathbb{I}} \quad (18)$$

*Proof.* See the Appendix in [7]. ■

**Definition 1.** Define the following non-attractive and forward invariant unstable set  $\mathcal{U}_s \subseteq \mathbb{SO}(3)$ :

$$\mathcal{U}_s = \{R(0) \in \mathbb{SO}(3) \mid \text{Tr}\{R(0)\} = -1\} \quad (19)$$

where  $R(0) \in \mathcal{U}_s$  in one of the following three cases:  $R(0) = \text{diag}(-1, -1, 1)$ ,  $R(0) = \text{diag}(-1, 1, -1)$ , or  $R(0) = \text{diag}(1, -1, -1)$ .

The goal of this work is two-fold and includes proposing a nonlinear observer and a controller which are strongly coupled and designed to operate as a module. Our first objective (Section IV) is to design a nonlinear observer able to estimate attitude ( $\hat{R}$ ), angular velocity ( $\hat{\Omega}$ ), position ( $\hat{P}$ ), and linear velocity ( $\hat{V}$ ) of a UAVs in six degrees of freedom (6 DoF) using onboard sensor measurements. Herein, measurements refer to feature information extracted from photos taken by a monocular or stereo camera. The proposed solution does

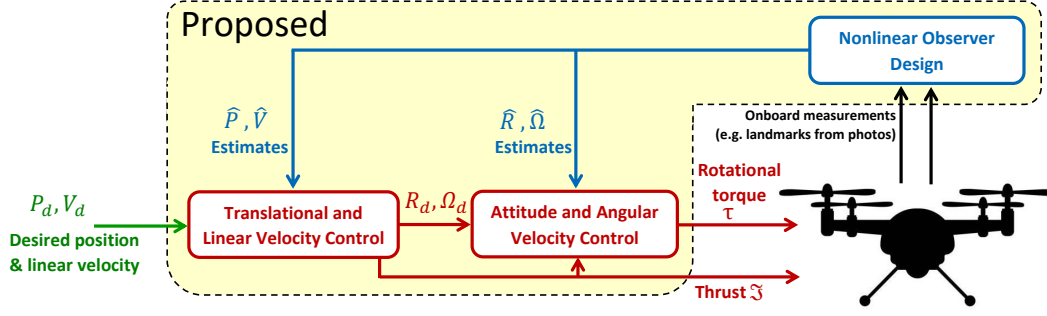


Fig. 2. Graphical summary of the proposed observer-based control solution for a VTOL-UAV.

not require an IMU or a GPS, but can be integrated with IMU and GPS measurements if needed. The second objective (Section V) is to design a controller that uses components estimated by the observer to generate rotational torque ( $\mathcal{T}$ ) and thrust ( $\mathfrak{S}$ ) necessary to control the VTOL-UAV with respect to a desired position and linear velocity trajectories. Fig. 2 graphically illustrates the research objective of this work.

#### IV. NONLINEAR OBSERVER DESIGN ON LIE GROUP

Define  $P_y \in \mathbb{R}^3$  as a reconstructed position and  $R_y \in \mathbb{SO}(3)$  as a reconstructed attitude of a VTOL-UAV (for more details visit [7], [8]). The concept of reconstruction is detailed in Section VII. For the sake of stability analysis of the observer design, it is considered that the reconstructed components  $P_y$  and  $R_y$  are close to the true components  $P$  and  $R$ . In the implementation, on the contrary, the observer is tested against a high level of uncertainties corrupting  $P_y$  and  $R_y$ . Define  $\hat{R} \in \mathbb{SO}(3)$ ,  $\hat{\Omega} \in \mathbb{R}^3$ ,  $\hat{P} \in \mathbb{R}^3$ , and  $\hat{V} \in \mathbb{R}^3$  as the estimates of the true attitude  $R \in \mathbb{SO}(3)$ , angular velocity  $\Omega \in \mathbb{R}^3$ , position  $P \in \mathbb{R}^3$ , and linear velocity  $V \in \mathbb{R}^3$ , respectively. Define the errors between the estimated and the true values of attitude, angular velocity, position, and linear velocity as

$$\tilde{R}_o = R\hat{R}^\top \quad (20)$$

$$\tilde{\Omega}_o = \Omega - \tilde{R}_o\hat{\Omega} \quad (21)$$

$$\tilde{P}_o = P - \hat{P} \quad (22)$$

$$\tilde{V}_o = V - \hat{V} \quad (23)$$

where  $\tilde{R}_o \in \mathbb{SO}(3)$ ,  $\tilde{\Omega}_o \in \mathbb{R}^3$ ,  $\tilde{P}_o \in \mathbb{R}^3$ , and  $\tilde{V}_o \in \mathbb{R}^3$ . Consider the nonlinear dynamics  $\dot{X} = XU - \mathcal{G}X \in T_X\mathbb{SE}_2(3)$  in (14) where  $X \in \mathbb{SE}_2(3)$  and  $U, \mathcal{G} \in \mathcal{U}_{\mathcal{M}}$  such that  $\mathbb{SE}_2(3) \times \mathcal{U}_{\mathcal{M}} \rightarrow T_X\mathbb{SE}_2(3)$ . The objective of this Section is to propose a nonlinear observer on the Lie group of  $\mathbb{SE}_2(3)$  that mimics the nonlinear dynamics in (14) with  $\hat{X} \in \mathbb{SE}_2(3)$  being the estimate of  $X$  such that  $\dot{\hat{X}} \in T_{\hat{X}}\mathbb{SE}_2(3)$ . The proposed observer aims to drive

$$\hat{R} \rightarrow R$$

$$\hat{\Omega} \rightarrow \Omega$$

$$\hat{P} \rightarrow P$$

$$\hat{V} \rightarrow V$$

with  $\lim_{t \rightarrow \infty} \tilde{R}_o = \mathbf{I}_3$  and  $\lim_{t \rightarrow \infty} \tilde{\Omega}_o = \lim_{t \rightarrow \infty} \tilde{P}_o = \lim_{t \rightarrow \infty} \tilde{V}_o = \mathbf{0}_{3 \times 1}$ . Let us propose a nonlinear observer for VTOL-UAV on Lie group in a compact form:

$$\begin{cases} \dot{\hat{X}} &= \hat{X}\hat{U} - W\hat{X} \\ \dot{\hat{J}}\hat{\Omega} &= [\hat{J}\hat{\Omega}]_{\times}\hat{\Omega} + \hat{\mathcal{T}} - \hat{J}[\hat{\Omega}]_{\times}\hat{R}w_{\Omega} + w_o \end{cases} \quad (24)$$

with the following set of correction factors:

$$\begin{cases} w_o &= -\gamma_o\tilde{R}_o^\top \mathbf{vex}(\mathcal{P}_a(\tilde{R}_o)), \quad \tilde{R}_o = R_y\hat{R}^\top \\ w_{\Omega} &= k_{o1}R_y^\top \mathbf{vex}(\mathcal{P}_a(\tilde{R}_o)) \\ w_V &= -[w_{\Omega}]_{\times}\hat{P} - k_{o2}\tilde{P}_o, \quad \tilde{P}_o = P_y - \hat{P} \\ w_a &= -\frac{\mathfrak{S}}{m}\hat{R}^\top(\mathbf{I}_3 - \tilde{R}_o^\top)e_3 - ge_3 - [w_{\Omega}]_{\times}\hat{V} - k_{o3}\tilde{P}_o \end{cases} \quad (25)$$

such that

$$\hat{X} = \mathcal{N}(\hat{R}^\top, \hat{P}, \hat{V}) = \begin{bmatrix} \hat{R}^\top & \hat{P} & \hat{V} \\ 0_{1 \times 3} & 1 & 0 \\ 0_{1 \times 3} & 0 & 1 \end{bmatrix} \in \mathbb{SE}_2(3)$$

in accordance with the map in (7),

$$\hat{U} = \underbrace{\begin{bmatrix} [\hat{\Omega}]_{\times} & 0_{3 \times 1} & -\frac{\mathfrak{S}}{m}e_3 \\ 0_{1 \times 3} & 0 & 0 \\ 0_{1 \times 3} & 1 & 0 \end{bmatrix}}_{u([\hat{\Omega}]_{\times}, 0_{3 \times 1}, -\frac{\mathfrak{S}}{m}e_3, 1)} \in \mathcal{U}_m$$

and

$$W = u([w_{\Omega}]_{\times}, w_V, w_a, 1) = \begin{bmatrix} [w_{\Omega}]_{\times} & w_V & w_a \\ 0_{1 \times 3} & 0 & 0 \\ 0_{1 \times 3} & 1 & 0 \end{bmatrix} \in \mathcal{U}_m$$

as per the map in (8),  $J$ ,  $m$ , and  $g$  denote vehicle's inertia matrix, mass, and gravitational acceleration, respectively,  $\hat{\mathcal{T}} = \tilde{R}_o^\top \mathcal{T}$  and  $\hat{J} = \tilde{R}_o^\top J \tilde{R}_o$  denote the rotational torque input and the inertia matrix, respectively, and  $\gamma_o$ ,  $k_{o1}$ ,  $k_{o2}$ , and  $k_{o3}$  stand for strictly positive constants. It becomes apparent that  $\dot{\hat{X}} \in T_{\hat{X}}\mathbb{SE}_2(3)$ . The detailed representation of the novel nonlinear observer in (24) is as follows:

$$\dot{\hat{R}} = \hat{R}[w_{\Omega}]_{\times} - [\hat{\Omega}]_{\times}\hat{R} \quad (26)$$

$$\dot{\hat{J}}\hat{\Omega} = [\hat{J}\hat{\Omega}]_{\times}\hat{\Omega} + \hat{\mathcal{T}} - \hat{J}[\hat{\Omega}]_{\times}\hat{R}w_{\Omega} + w_o \quad (27)$$

$$\dot{\hat{P}} = \hat{V} - [w_{\Omega}]_{\times}\hat{P} - w_V \quad (28)$$

$$\dot{\hat{V}} = -\frac{\mathfrak{S}}{m}\hat{R}^\top e_3 - [w_{\Omega}]_{\times}\hat{V} - w_a \quad (29)$$

**Theorem 1.** Consider VTOL-UAV dynamics in (12) and (13), and suppose that Assumption 1 is satisfied. Couple the inertial and landmark measurements  $y_i^B = Rv_i^T$  and  $z_j^B = R(p_j^T - P)$  for all  $i = 1, 2, \dots, N_1$  and  $j = 1, 2, \dots, N_2$  with the observer in (24) and the correction factors in (25). Let  $\gamma_o$ ,  $k_{o1}$ ,  $k_{o2}$ , and  $k_{o3}$  be positive constants and  $\tilde{R}_o(0) \notin \mathcal{U}_s$  (see Definition 1). Define the set:

$$\mathcal{S}_o = \{(\tilde{R}_o, \tilde{\Omega}_o, \tilde{P}_o, \tilde{V}_o) \in \mathbb{SO}(3) \times \mathbb{R}^3 \times \mathbb{R}^3 \times \mathbb{R}^3 \mid \tilde{R}_o = \mathbf{I}_3, \tilde{\Omega}_o = \tilde{P}_o = \tilde{V}_o = \mathbf{0}_{3 \times 1}\} \quad (30)$$

Then, the set  $\mathcal{S}_o$  is uniformly almost globally exponentially stable.

*Proof.* It is stated in Theorem 1 that error signals converge exponentially to the equilibrium point from any initial condition except for the three repeller orientations defined in Definition 1 ( $\tilde{R}_o(0) \notin \mathcal{U}_s$ ). Consider the attitude error  $\tilde{R}_o = R\hat{R}^T$  in (20). From (12) and (26), one has

$$\begin{aligned} \dot{\tilde{R}}_o &= \dot{R}\hat{R}^T + R\dot{\hat{R}}^T \\ &= -[\Omega]_{\times} R\hat{R}^T + R(-[w_{\Omega}]_{\times} \hat{R}^T + \hat{R}^T [\hat{\Omega}]_{\times}) \\ &= -[\Omega]_{\times} \tilde{R}_o + \tilde{R}_o [\hat{\Omega}]_{\times} - [Rw_{\Omega}]_{\times} \tilde{R}_o \\ &= -[\Omega - \tilde{R}_o \hat{\Omega} + Rw_{\Omega}]_{\times} \tilde{R}_o = -[\tilde{\Omega}_o + Rw_{\Omega}]_{\times} \tilde{R}_o \end{aligned} \quad (31)$$

where  $\tilde{\Omega}_o$  is defined in (21). Using (4) and (31), one obtains [7]

$$\begin{aligned} \|\dot{\tilde{R}}_o\|_I &= -\frac{1}{4} \text{Tr}\{\dot{\tilde{R}}_o\} = \frac{1}{4} \text{Tr}\{[\tilde{\Omega}_o + Rw_{\Omega}]_{\times} \mathcal{P}_a(\tilde{R}_o)\} \\ &= -\frac{1}{2} \text{vex}(\mathcal{P}_a(\tilde{R}_o))^{\top} (\tilde{\Omega}_o + Rw_{\Omega}) \end{aligned} \quad (32)$$

From (12), (21), (27), and (31), one finds

$$\begin{aligned} J\dot{\tilde{\Omega}}_o &= J\dot{\Omega} - J\dot{\tilde{R}}_o \hat{\Omega} - J\tilde{R}_o \dot{\hat{\Omega}} \\ &= [J\Omega]_{\times} \Omega + \mathcal{T} + J[\tilde{\Omega}_o + Rw_{\Omega}]_{\times} \tilde{R}_o \hat{\Omega} - J\tilde{R}_o \dot{\hat{\Omega}} \\ &= [J\Omega]_{\times} \Omega + J[\tilde{\Omega}_o]_{\times} \tilde{R}_o \hat{\Omega} - [J\tilde{R}_o \hat{\Omega}]_{\times} \tilde{R}_o \hat{\Omega} \\ &\quad \mathcal{T} + [J\tilde{R}_o \hat{\Omega}]_{\times} \tilde{R}_o \hat{\Omega} + J[Rw_{\Omega}]_{\times} \tilde{R}_o \hat{\Omega} - \tilde{R}_o J\dot{\hat{\Omega}} \\ &= S(\Omega) \tilde{\Omega}_o - [J\tilde{\Omega}_o]_{\times} \tilde{\Omega}_o - \tilde{R}_o w_o \end{aligned} \quad (33)$$

such that

$$\begin{aligned} [J\Omega]_{\times} \Omega + J[\tilde{\Omega}_o]_{\times} \tilde{R}_o \hat{\Omega} - [J\tilde{R}_o \hat{\Omega}]_{\times} \tilde{R}_o \hat{\Omega} \\ &= [J\Omega]_{\times} \Omega + (J[\tilde{\Omega}_o]_{\times} - [J\Omega]_{\times} + [J\tilde{\Omega}_o]_{\times}) \tilde{R}_o \hat{\Omega} \\ &= [J\Omega]_{\times} \tilde{\Omega}_o - J[\Omega]_{\times} \tilde{\Omega}_o - [\Omega]_{\times} J\tilde{\Omega}_o - [J\tilde{\Omega}_o]_{\times} \tilde{\Omega}_o \\ &= ([J\Omega]_{\times} - J[\Omega]_{\times} - [\Omega]_{\times} J) \tilde{\Omega}_o - [J\tilde{\Omega}_o]_{\times} \tilde{\Omega}_o \\ &= S(\Omega) \tilde{\Omega}_o - [J\tilde{\Omega}_o]_{\times} \tilde{\Omega}_o \end{aligned} \quad (34)$$

where  $S(\Omega) = [J\Omega]_{\times} - J[\Omega]_{\times} - [\Omega]_{\times} J \in \mathfrak{so}(3)$ ,  $[\Omega]_{\times} \tilde{\Omega}_o = -[\tilde{\Omega}_o]_{\times} \Omega$ , and the identity in (10) is employed. From (13), (22), and (28), one obtains

$$\dot{\tilde{P}}_o = \tilde{V}_o - k_{o2} \tilde{P}_o \quad (35)$$

From (13), (23), and (29), one has

$$\dot{\tilde{V}}_o = -k_{o3} \tilde{P}_o \quad (36)$$

Define the following cost function  $L_1 : \mathbb{SO}(3) \times \mathbb{R}^3 \rightarrow \mathbb{R}_+$ :

$$L_1 = 2\|\tilde{R}_o\|_I + \frac{1}{2\gamma_o} \tilde{\Omega}_o^{\top} J \tilde{\Omega}_o \quad (37)$$

In view of (32), (33), and the correction factors  $w_{\Omega}$  and  $w_o$  in (25), one finds that the derivative of (37) is as follows:

$$\begin{aligned} \dot{L}_1 &= -\text{vex}(\mathcal{P}_a(\tilde{R}_o))^{\top} (\tilde{\Omega}_o + Rw_{\Omega}) \\ &\quad + \frac{1}{\gamma_o} \tilde{\Omega}_o^{\top} (S(\Omega) \tilde{\Omega}_o - [J\tilde{\Omega}_o]_{\times} \tilde{\Omega}_o - \tilde{R}_o w_o) \\ &= -k_{o1} \|\text{vex}(\mathcal{P}_a(\tilde{R}_o))\|^2 \end{aligned} \quad (38)$$

where  $[\tilde{\Omega}_o]_{\times} \tilde{\Omega}_o = \mathbf{0}_{3 \times 1}$ . It becomes clear that  $\dot{L}_1$  is negative, continuous, and strictly decreasing, and consequently,  $L_1$  is bounded indicating that  $\text{vex}(\mathcal{P}_a(\tilde{R}_o))$  and  $\tilde{\Omega}_o$  are also bounded. Hence,  $\dot{L}_1$  is bounded, and according to Barbalat Lemma,  $\lim_{t \rightarrow \infty} \text{vex}(\mathcal{P}_a(\tilde{R}_o)) = \mathbf{0}_{3 \times 1}$  shows that  $\|\tilde{R}_o\|_I \rightarrow 0$ ,  $\|\dot{\tilde{R}}_o\|_I \rightarrow 0$ ,  $\lim_{t \rightarrow \infty} \tilde{R}_o = \mathbf{0}_{3 \times 3}$ ,  $\lim_{t \rightarrow \infty} \tilde{R}_o = \mathbf{I}_3$ , and  $\lim_{t \rightarrow \infty} w_{\Omega} = \lim_{t \rightarrow \infty} w_o = \mathbf{0}_{3 \times 1}$ . Hence,  $\lim_{t \rightarrow \infty} \tilde{\Omega}_o = \mathbf{0}_{3 \times 1}$ , and thereby,  $\lim_{t \rightarrow \infty} L_1 = 0$ . The derivative of the vex operator is equivalent to [32]

$$\text{vex}(\mathcal{P}_a(\tilde{R}_o)) = -\frac{1}{2} \Psi(\tilde{R}_o) (\tilde{\Omega}_o + Rw_{\Omega}) \quad (39)$$

where  $\Psi(\tilde{R}_o) = \text{Tr}\{\tilde{R}_o\} \mathbf{I}_3 - \tilde{R}_o$ . Recalling Lemma 1, (39) and (33), one has

$$\begin{aligned} \frac{1}{2\delta_{o1}} \frac{d}{dt} \text{vex}(\mathcal{P}_a(\tilde{R}_o))^{\top} \tilde{\Omega}_o &= -\frac{1}{4\delta_{o1}} (\tilde{\Omega}_o + Rw_{\Omega})^{\top} \Psi(\tilde{R}_o) \tilde{\Omega}_o \\ &\quad + \frac{1}{2\delta_{o1}} \text{vex}(\mathcal{P}_a(\tilde{R}_o))^{\top} J^{-1} (S(\Omega) \tilde{\Omega}_o - [J\tilde{\Omega}_o]_{\times} \tilde{\Omega}_o - \tilde{R}_o w_o) \\ &\leq -\frac{2\gamma_o c_{o3}}{\delta_{o1}} \|\tilde{R}_o\|_I - \frac{1}{4\delta_{o1}} \|\tilde{\Omega}_o\|^2 + \frac{c_{o2}}{2\delta_{o1}} \|\tilde{\Omega}_o\| \sqrt{\|\tilde{R}_o\|_I} \end{aligned} \quad (40)$$

where  $\delta_{o1}$  is a positive constant,  $\eta_{\Omega} = \sup_{t \geq 0} S(\Omega)$ ,  $c_{o1} = 2\sqrt{1 - \|\tilde{R}_o(0)\|_I}$ ,  $c_{o2} = \frac{c_{o1}(2\eta_{\Omega} + \lambda_J \eta_{\Omega} + 3\lambda_J k_{o1}) + 0.5\eta_{\Omega}}{\lambda_J}$ , and  $c_{o3} = \frac{c_{o1}^2}{\lambda_J}$ . In view of  $L_1$  in (37), define the following Lyapunov function candidate  $\mathcal{L}_{o1} : \mathbb{SO}(3) \times \mathbb{R}^3 \rightarrow \mathbb{R}_+$ :

$$\mathcal{L}_{o1} = 2\|\tilde{R}_o\|_I + \frac{1}{2\gamma_o} \tilde{\Omega}_o^{\top} J \tilde{\Omega}_o + \frac{1}{2\delta_{o1}} \text{vex}(\mathcal{P}_a(\tilde{R}_o))^{\top} \tilde{\Omega}_o \quad (41)$$

Based on Lemma 1, one finds

$$e_{o1}^{\top} \left[ \underbrace{\begin{bmatrix} 2 & -\frac{\lambda_J c_{o1}}{4\delta_{o1}} \\ -\frac{\lambda_J c_{o1}}{4\delta_{o1}} & \frac{\lambda_J}{2\gamma_o} \end{bmatrix}}_{M_1} e_{o1} \leq \mathcal{L}_{o1} \leq e_{o1}^{\top} \left[ \underbrace{\begin{bmatrix} 2 & \frac{\lambda_J c_{o1}}{4\delta_{o1}} \\ \frac{\lambda_J c_{o1}}{4\delta_{o1}} & \frac{\lambda_J}{2\gamma_o} \end{bmatrix}}_{M_2} e_{o1} \right]$$

where  $e_{o1} = [\sqrt{\|\tilde{R}_o\|_I}, \|\tilde{\Omega}_o\|]^{\top}$ . The matrices  $M_1$  and  $M_2$  can be made positive by selecting  $\delta_{o1} > \frac{\lambda_J c_{o1}}{4} \sqrt{\frac{\gamma_o}{\lambda_J}}$ . Therefore, from (37), (38), and (40), the derivative of (41) becomes

$$\dot{\mathcal{L}}_{o1} \leq -\frac{1}{4\delta_{o1}} e_{o1}^{\top} \underbrace{\begin{bmatrix} 8(k_{o1} \delta_{o1} - \gamma_o c_{o3}) & c_{o2} \\ c_{o2} & 1 \end{bmatrix}}_{A_{o1}} e_{o1} \quad (42)$$

$A_{o1}$  can be made positive by selecting  $\delta_{o1} > \frac{c_{o2}^2 - \gamma_o c_{o3}}{8k_{o1}}$ . By selecting  $\delta_{o1} > \max\{\frac{\lambda_J c_{o1}}{4} \sqrt{\frac{\gamma_o}{\lambda_J}}, \frac{c_{o2}^2 + \gamma_o c_{o3}}{8k_{o1}}\}$  and defining  $\underline{\lambda}_{A_{o1}}$  as the minimum eigenvalue of  $A_{o1}$ , one has

$$\dot{\mathcal{L}}_{o1} \leq -\underline{\lambda}_{A_{o1}} \|\tilde{R}_o\|_I - \underline{\lambda}_{A_{o1}} \|\tilde{\Omega}_o\|^2 \quad (43)$$

Consider the following Lyapunov function candidate  $\mathcal{L}_{o2} : \mathbb{R}^3 \times \mathbb{R}^3 \rightarrow \mathbb{R}_+$ :

$$\mathcal{L}_{o2} = \frac{1}{2} \tilde{P}_o^\top \tilde{P}_o + \frac{1}{2k_{o3}} \tilde{V}_o^\top \tilde{V}_o - \delta_{o2} \tilde{P}_o^\top \tilde{V}_o \quad (44)$$

It can be easily shown that  $\mathcal{L}_{o2}$  follows

$$e_{o2}^\top \underbrace{\begin{bmatrix} \frac{1}{2} & -\frac{\delta_{o2}}{2} \\ -\frac{\delta_{o2}}{2} & \frac{1}{2k_{o3}} \end{bmatrix}}_{M_3} e_{o2} \leq \mathcal{L}_{o2} \leq e_{o2}^\top \underbrace{\begin{bmatrix} \frac{1}{2} & \frac{\delta_{o2}}{2} \\ \frac{\delta_{o2}}{2} & \frac{1}{2k_{o3}} \end{bmatrix}}_{M_4} e_{o2}$$

where  $e_{o2} = [||\tilde{P}_o||, ||\tilde{V}_o||]^\top$ . It is evident that  $M_3$  and  $M_4$  are positive if  $\delta_{o2} < \frac{1}{\sqrt{k_{o3}}}$ . From (35) and (36), one finds

$$\begin{aligned} \dot{\mathcal{L}}_{o2} &= -k_{o2} \tilde{P}_o^\top \tilde{P}_o - \delta_{o2} \tilde{V}_o^\top \tilde{V}_o + \delta_{o2} k_{o2} \tilde{P}_o^\top \tilde{V}_o + \delta_{o2} k_{o3} \tilde{P}_o^\top \tilde{P}_o \\ &\leq -e_{o2}^\top \underbrace{\begin{bmatrix} (k_{o2} - \delta_{o2} k_{o3}) & \frac{k_{o2} \delta_{o2}}{2} \\ \frac{k_{o2} \delta_{o2}}{2} & \delta_{o2} \end{bmatrix}}_{A_{o2}} e_{o2} \end{aligned} \quad (45)$$

It becomes apparent that  $A_{o2}$  is made positive by selecting  $\delta_{o2} < \frac{4k_{o2}}{k_{o2}^2 + k_{o3}}$ . By selecting  $\delta_{o2} < \min\{\frac{1}{\sqrt{k_{o3}}}, \frac{4k_{o2}}{k_{o2}^2 + k_{o3}}\}$  and defining  $\lambda_{A_{o2}}$  as the minimum eigenvalue of  $A_{o2}$ , one shows that

$$\dot{\mathcal{L}}_{o2} \leq -\lambda_{A_{o2}} (||\tilde{P}_o||^2 + ||\tilde{V}_o||^2) \quad (46)$$

From (41) and (44), let us define the total Lyapunov function candidate for the observer design  $\mathcal{L}_{oT} : \mathbb{SO}(3) \times \mathbb{R}^3 \times \mathbb{R}^3 \times \mathbb{R}^3 \rightarrow \mathbb{R}_+$  as follows:

$$\mathcal{L}_{oT} = \mathcal{L}_{o1} + \mathcal{L}_{o2} \quad (47)$$

From (43) and (45), one obtains

$$\dot{\mathcal{L}}_{oT} \leq -\lambda_{A_o} (||\tilde{R}_o||_1 + ||\tilde{\Omega}_o||^2 + ||\tilde{P}_o||^2 + ||\tilde{V}_o||^2) \quad (48)$$

with  $\lambda_{A_o} = \min\{\lambda_{A_{o1}}, \lambda_{A_{o2}}\}$ . Define  $\eta_o = \max\{\bar{\lambda}(M_1), \bar{\lambda}(M_2), \bar{\lambda}(M_3), \bar{\lambda}(M_4)\}$ . From (41), (44), (43), (46), (47), and (48), the following inequality is obtained:

$$\mathcal{L}_{oT}(t) \leq \mathcal{L}_{oT}(0) \exp(-\lambda_{A_o} t / \eta_o) \quad (49)$$

such that  $\lim_{t \rightarrow \infty} \tilde{R}_o = \mathbf{I}_3$ ,  $\lim_{t \rightarrow \infty} \tilde{\Omega}_o = \mathbf{0}_{3 \times 1}$ ,  $\lim_{t \rightarrow \infty} \tilde{P}_o = \mathbf{0}_{3 \times 1}$ , and  $\lim_{t \rightarrow \infty} \tilde{V}_o = \mathbf{0}_{3 \times 1}$  exponentially. Consequently, the closed loop error signals of the observer design are uniformly almost globally exponentially stable and converge to the set  $\mathcal{S}_o$  proving Theorem 1. ■

## V. OBSERVER-BASED CONTROLLER SCHEME

As has been mentioned in the Introduction section, most of the existing VTOL-UAV observer-based controllers utilize Euler angles representation which is subject to singularity and fails to represent the attitude at several configurations. Singularity of these methods leads to local results. In addition, studies that use unit-quaternion suffer from non-uniqueness in the attitude representation. This work, on the contrary, designs the observer and the control laws using a Lie Group matrix form which allows for unique and global attitude representation. The objective of this Section is to design almost global control laws for torque  $\mathcal{T} \in \mathbb{R}^3$  and thrust  $\mathfrak{S} \in \mathbb{R}$  to accurately track the VTOL-UAV position and velocity along the desired trajectories using the estimates from Section IV:  $\tilde{R}$ ,  $\tilde{\Omega}$ ,  $\tilde{P}$ , and  $\tilde{V}$ . Define  $R_d \in \mathbb{SO}(3)$ ,  $\Omega_d \in \mathbb{R}^3$ ,  $P_d \in \mathbb{R}^3$ , and  $V_d \in \mathbb{R}^3$

as the VTOL-UAV desired attitude, angular velocity, position, and linear velocity, respectively. The proposed control strategy aims to drive

$$R \rightarrow R_d$$

$$\Omega \rightarrow \Omega_d$$

$$P \rightarrow P_d$$

$$V \rightarrow V_d$$

Hence, define the errors in attitude, angular velocity, position, and linear velocity as

$$\tilde{R}_c = R R_d^\top \quad (50)$$

$$\tilde{\Omega}_c = \Omega - \tilde{R}_c \Omega_d \quad (51)$$

$$\tilde{P}_c = P - P_d \quad (52)$$

$$\tilde{V}_c = V - V_d \quad (53)$$

where  $\tilde{R}_c \in \mathbb{SO}(3)$ ,  $\tilde{\Omega}_c \in \mathbb{R}^3$ ,  $\tilde{P}_c \in \mathbb{R}^3$ , and  $\tilde{V}_c \in \mathbb{R}^3$ . The proposed control laws aim to achieve  $\lim_{t \rightarrow \infty} \tilde{R}_c = \mathbf{I}_3$  and  $\lim_{t \rightarrow \infty} \tilde{\Omega}_c = \lim_{t \rightarrow \infty} \tilde{P}_c = \lim_{t \rightarrow \infty} \tilde{V}_c = \mathbf{0}_{3 \times 1}$ . Based on (12), the desired attitude dynamics are as follows:

$$\dot{R}_d = -[\Omega_d]_\times R_d \quad (54)$$

Rewrite the velocity dynamics  $\dot{V} = g e_3 - \frac{\mathfrak{S}}{m} R^\top e_3$  in (13) as

$$\begin{aligned} \dot{V} &= g e_3 - \frac{\mathfrak{S}}{m} R_d^\top e_3 - \frac{\mathfrak{S}}{m} (R^\top - R_d^\top) e_3 \\ &= F - \frac{\mathfrak{S}}{m} (R^\top - R_d^\top) e_3 \end{aligned}$$

where  $F$  denotes an intermediary control input defined by

$$F = g e_3 - \frac{\mathfrak{S}}{m} R_d^\top e_3 = [f_1, f_2, f_3]^\top \in \mathbb{R}^3 \quad (55)$$

Consequently,  $\mathfrak{S} = m ||g e_3 - F||$ .

**Lemma 2.** [33] Consider the dynamics in (13) and the intermediary control input in (55) with thrust magnitude  $\mathfrak{S} = m ||g e_3 - F||$ . The desired unit-quaternion components  $Q_d = [q_{d0}, q_d^\top]^\top \in \mathbb{S}^3$  are as follows:

$$q_{d0} = \sqrt{\frac{m}{2\mathfrak{S}}(g - f_3) + \frac{1}{2}}, \quad q_d = \begin{bmatrix} \frac{m}{2\mathfrak{S}q_{d0}} f_2 \\ -\frac{m}{2\mathfrak{S}q_{d0}} f_1 \\ 0 \end{bmatrix} \quad (56)$$

on condition that  $F \neq [0, 0, a]^\top$  for  $a \geq g$ . Note that  $\mathbb{S}^3 = \{Q_d \in \mathbb{R}^4 | ||Q_d|| = 1\}$  (see Subsection II-C). Let  $F$  be differentiable with the desired angular velocity defined as

$$\Omega_d = \Xi(F) \dot{F} \quad (57)$$

and

$$\Xi(F) = \frac{1}{\alpha_1^2 \alpha_2} \begin{bmatrix} -f_1 f_2 & -f_2^2 + \alpha_1 \alpha_2 & f_2 \alpha_2 \\ f_1^2 - \alpha_1 \alpha_2 & f_1 f_2 & -f_1 \alpha_2 \\ f_2 \alpha_1 & -f_1 \alpha_1 & 0 \end{bmatrix} \quad (58)$$

where  $\alpha_1 = ||g e_3 - F||$  and  $\alpha_2 = ||g e_3 - F|| + g - f_3$ . ■

From Lemma 2 and given the desired unit-quaternion  $Q_d = [q_{d0}, q_d^\top]^\top \in \mathbb{S}^3$ , the desired attitude  $R_d = \mathcal{R}_{Q_d}$  can be obtained from the map in (9) as follows:

$$\mathcal{R}_{Q_d} = (q_{d0}^2 - ||q_d||^2) \mathbf{I}_3 + 2q_d q_d^\top - 2q_{d0} [q_d]_\times \in \mathbb{SO}(3)$$

It is worth noting that Lemma 2 indicates that  $Q_d$  and  $\mathfrak{S}$  are singularity-free.

**Remark 1.** In this work  $F$  is designed to be twice differentiable such that the desired angular velocity rate of change  $\dot{\Omega}_d$  can be defined as

$$\dot{\Omega}_d = \dot{\Xi}(F)\dot{F} + \Xi(F)\ddot{F} \quad (59)$$

$\dot{F}$  and  $\ddot{F}$  are provided in the Appendix.

Let us define the following variables:

$$\mathcal{E} = \tilde{P}_c - \theta, \quad \dot{\mathcal{E}} = \tilde{V}_c - \dot{\theta} \quad (60)$$

where  $\theta \in \mathbb{R}^3$  stands for an auxiliary variable. Consider proposing the following VTOL-UAV control strategy:

$$\begin{aligned} \mathcal{T} = & k_{c1} \text{vex}(\mathcal{P}_a(\tilde{R}_c)) - k_{c2}(\tilde{R}_o\hat{\Omega} - \tilde{R}_c\Omega_d) + J\tilde{R}_c\dot{\Omega}_d \\ & + [\tilde{R}_c\Omega_d]_{\times} J\tilde{R}_c\Omega_d \end{aligned} \quad (61)$$

$$\begin{aligned} \ddot{\theta} = & -k_{\theta 1}\psi(\theta) - k_{\theta 2}\psi(\dot{\theta}) + k_{c3}(\hat{P} - P_d - \theta) \\ & + k_{c4}(\hat{V} - V_d - \dot{\theta}) \end{aligned} \quad (62)$$

$$F = \ddot{P}_d - k_{\theta 1}\psi(\theta) - k_{\theta 2}\psi(\dot{\theta}) \quad (63)$$

$$\mathfrak{S} = m\|ge_3 - F\| \quad (64)$$

where  $\mathcal{T}$  denotes the torque input,  $J$  denotes the inertia matrix of the vehicle,  $\tilde{R}_o = R_y\hat{R}^\top$ ,  $\tilde{R}_c = R_yR_d^\top$ ,  $R_y$  represents the reconstructed attitude,  $\theta \in \mathbb{R}^3$  stands for an auxiliary variable,  $F$  denotes the intermediary control input (selected as in [34]),  $g$  and  $m$  are defined in (13),  $\mathfrak{S} \in \mathbb{R}$  is the magnitude of thrust,  $\hat{\Omega}$ ,  $\hat{P}$ , and  $\hat{V}$  denote the estimates of angular velocity, position, and linear velocity, respectively,  $\ddot{P}_d$  denotes the second derivative of the desired position,  $\psi(\theta)$  and  $\psi(\dot{\theta})$  are the bounded functions defined in the Appendix, and  $k_{\theta 1}$ ,  $k_{\theta 2}$ ,  $k_{c1}$ ,  $k_{c2}$ ,  $k_{c3}$ , and  $k_{c4}$  are strictly positive constants.

**Theorem 2.** Consider combining the true VTOL-UAV nonlinear dynamics in (12) and (13) and the nonlinear observer in (24) with the control laws in (61) and (64). Let Assumption 2 hold and let  $\tilde{R}_c(0) \notin \mathcal{U}_s$ . Define the following set:

$$\begin{aligned} \mathcal{S}_c = & \{(\tilde{R}_c, \tilde{\Omega}_c, \tilde{P}_c, \tilde{V}_c) \in \text{SO}(3) \times \mathbb{R}^3 \times \mathbb{R}^3 \times \mathbb{R}^3 \mid \\ & \tilde{R}_c = \mathbf{I}_3, \tilde{\Omega}_c = \tilde{P}_c = \tilde{V}_c = \mathbf{0}_{3 \times 1}\} \end{aligned} \quad (65)$$

Then, the set  $\mathcal{S}_c$  is uniformly almost globally exponentially stable.

*Proof.* The statement in Theorem 2 entails that the closed loop error signals converge exponentially to the equilibrium point starting from any initial condition except for the three repeller attitude cases given in Definition 1 ( $\tilde{R}_c(0) \notin \mathcal{U}_s$ ). Consider the attitude error  $\tilde{R}_c = RR_d^\top$  in (50). Using (12) and (54), one shows that

$$\begin{aligned} \dot{\tilde{R}}_c = & R\dot{R}_d^\top + \dot{R}R_d^\top = \tilde{R}_c[\Omega_d]_{\times} - [\Omega]_{\times}\tilde{R}_c \\ = & -[\Omega - \tilde{R}_c\Omega_d]_{\times}\tilde{R}_c = -[\tilde{\Omega}_c]_{\times}\tilde{R}_c \end{aligned} \quad (66)$$

where the identity in (10) was used, and  $\tilde{\Omega}_c$  is defined in (51). In view of (4), (11), and (66), one finds [7]

$$\begin{aligned} \|\dot{\tilde{R}}_c\|_{\text{I}} = & -\frac{1}{4}\text{Tr}\{\dot{\tilde{R}}_c\} = \frac{1}{4}\text{Tr}\{[\tilde{\Omega}_c]_{\times}\mathcal{P}_a(\tilde{R}_c)\} \\ = & -\frac{1}{2}\text{vex}(\mathcal{P}_a(\tilde{R}_c))^\top \tilde{\Omega}_c \end{aligned} \quad (67)$$

In view of (12), (51), and (66), one has

$$\begin{aligned} J\dot{\tilde{\Omega}}_c = & J\dot{\Omega} - J\dot{\tilde{R}}_c\Omega_d - J\tilde{R}_c\dot{\Omega}_d \\ = & [J\Omega]_{\times}\Omega + \mathcal{T} + J[\tilde{\Omega}_c]_{\times}\tilde{R}_c\Omega_d - J\tilde{R}_c\dot{\Omega}_d \\ = & S(\Omega)\tilde{\Omega}_c - [J\tilde{\Omega}_c]_{\times}\tilde{\Omega}_c + \mathcal{T} \\ & + [J\tilde{R}_c\Omega_d]_{\times}\tilde{R}_c\Omega_d - J\tilde{R}_c\dot{\Omega}_d \end{aligned} \quad (68)$$

with

$$\begin{aligned} [J\Omega]_{\times}\Omega + J[\tilde{\Omega}_c]_{\times}\tilde{R}_c\Omega_d - [J\tilde{R}_c\Omega_d]_{\times}\tilde{R}_c\Omega_d \\ = & [J\Omega]_{\times}\Omega + (J[\tilde{\Omega}_c]_{\times} - [J\Omega]_{\times} + [J\tilde{\Omega}_c]_{\times})\tilde{R}_c\Omega_d \\ = & [J\Omega]_{\times}\tilde{\Omega}_c - J[\Omega]_{\times}\tilde{\Omega}_c - [\Omega]_{\times}J\tilde{\Omega}_c - [J\tilde{\Omega}_c]_{\times}\tilde{\Omega}_c \\ = & S(\Omega)\tilde{\Omega}_c - [J\tilde{\Omega}_c]_{\times}\tilde{\Omega}_c \end{aligned} \quad (69)$$

using the fact that  $[\Omega]_{\times}\tilde{\Omega}_c = -[\tilde{\Omega}_c]_{\times}\Omega$  and  $S(\Omega) = [J\Omega]_{\times} - J[\Omega]_{\times} - [\Omega]_{\times}J \in \mathfrak{so}(3)$ . From (52) and (13), one has

$$\dot{\tilde{P}}_c = \tilde{V}_c \quad (70)$$

where  $\dot{P}_d = V_d$ . In the same spirit, from (53), (13), and (55), one shows that

$$\dot{\tilde{V}}_c = F - \|ge_3 - F\|(\tilde{R}^\top - R_d^\top)e_3 - \ddot{P}_d \quad (71)$$

Define the real-valued function  $L_2 : \text{SO}(3) \times \mathbb{R}^3 \rightarrow \mathbb{R}_+$

$$L_2 = 2\|\tilde{R}_c\|_{\text{I}} + \frac{1}{k_{c1}}\tilde{\Omega}_c^\top J\tilde{\Omega}_c \quad (72)$$

Considering (50), (51), and (61), the derivative of (72) is

$$\begin{aligned} \dot{L}_2 = & -\frac{1}{2}\text{vex}(\mathcal{P}_a(\tilde{R}_c))^\top \tilde{\Omega}_c \\ & + \frac{1}{k_{c3}}\tilde{\Omega}_c^\top(\mathcal{T} + [J\tilde{R}_c\Omega_d]_{\times}\tilde{R}_c\Omega_d - J\tilde{R}_c\dot{\Omega}_d) \\ \leq & -\frac{k_{c2}}{k_{c1}}\|\tilde{\Omega}_c\|^2 + \frac{k_{c2}}{k_{c1}}\|\tilde{\Omega}_c\|\|\tilde{\Omega}_o\| \end{aligned} \quad (73)$$

with  $[\tilde{\Omega}_c]_{\times}\tilde{\Omega}_c = \mathbf{0}_{3 \times 1}$ . It follows from (48) that  $\tilde{\Omega}_o$  is bounded and converges to zero. Hence,  $\tilde{\Omega}_c$  is bounded and  $\lim_{t \rightarrow \infty} \|\tilde{\Omega}_c\| = 0$ . Given that  $\tilde{\Omega}_o$ ,  $\tilde{\Omega}_c$ ,  $\Omega_d$ ,  $\tilde{\Omega}_d$ , and  $\dot{L}_2$  are bounded, consider the following derivative of the vex operator [32]:

$$\text{vex}(\mathcal{P}_a(\dot{\tilde{R}}_c)) = -\frac{1}{2}\Psi(\tilde{R}_c)\tilde{\Omega}_c \quad (74)$$

where  $\Psi(\tilde{R}_c) = \text{Tr}\{\tilde{R}_c\}\mathbf{I}_3 - \tilde{R}_c$ . Now, let us find the derivative

$$\begin{aligned} -\frac{1}{2\delta_{c1}}\frac{d}{dt}\text{vex}(\mathcal{P}_a(\dot{\tilde{R}}_c))^\top \tilde{\Omega}_c \\ \leq -\frac{k_{c1}c_{c2}}{2\delta_{c1}}\|\tilde{R}_c\|_{\text{I}} + \frac{c_{c3}\|\tilde{\Omega}_c\| + c_{c4}\|\tilde{\Omega}_o\|}{2\delta_{c1}}\sqrt{\|\tilde{R}_c\|_{\text{I}}} \end{aligned} \quad (75)$$

where  $\eta_{\Omega_c} = \sup_{t \geq 0} \|J\tilde{\Omega}_c\|$ ,  $\eta_{\Omega} = \sup_{t \geq 0} S(\Omega)$ ,  $c_{c1} = \sqrt{1 - \|\tilde{R}_c(0)\|_{\text{I}}}$ ,  $c_{c2} = \frac{c_{c1}^2}{\lambda_J}$ ,  $c_{c3} = \frac{(\eta_{\Omega} + k_{c2})c_{c1} + (1 + \lambda_J)\eta_{\Omega_c}}{\lambda_J}$ , and  $c_{c4} = \frac{k_{c2}c_{c1}}{\lambda_J}$ . Based on (72) and (75), consider the following Lyapunov function candidate  $\mathcal{L}_{c1} : \text{SO}(3) \times \mathbb{R}^3 \rightarrow \mathbb{R}_+$ :

$$\mathcal{L}_{c1} = 2\|\tilde{R}_c\|_{\text{I}} + \frac{1}{2k_{c1}}\tilde{\Omega}_c^\top J\tilde{\Omega}_c - \frac{1}{2\delta_{c1}}\text{vex}(\mathcal{P}_a(\tilde{R}_c))^\top \tilde{\Omega}_c \quad (76)$$



such that

$$e_{c1}^\top \underbrace{\begin{bmatrix} 2 & -\frac{\bar{\lambda}_J c_{c1}}{4\delta_{c1}} \\ -\frac{\bar{\lambda}_J c_{c1}}{4\delta_{c1}} & \frac{\lambda_J}{2k_{c1}} \end{bmatrix}}_{M_5} e_{c1} \leq \mathcal{L}_{c1} \leq e_{c1}^\top \underbrace{\begin{bmatrix} 2 & \frac{\bar{\lambda}_J c_{c1}}{4\delta_{c1}} \\ \frac{\bar{\lambda}_J c_{c1}}{4\delta_{c1}} & \frac{\lambda_J}{2k_{c1}} \end{bmatrix}}_{M_6} e_{c1}$$

where  $e_{c1} = [\sqrt{\|\tilde{R}_c\|_I}, \|\tilde{\Omega}_c\|]^\top$ .  $M_5$  and  $M_6$  are positive if  $\delta_{c1} > \frac{\bar{\lambda}_J c_{c1}}{4} \sqrt{\frac{k_{c1}}{\lambda_J}}$ . Based on (76), (73), and (75), one finds

$$\begin{aligned} \dot{\mathcal{L}}_{c1} \leq & -e_{c1}^\top \underbrace{\begin{bmatrix} \frac{k_{c1} c_{c2}}{2\delta_{c1}} & \frac{c_{c3}}{4\delta_{c1}} \\ \frac{c_{c3}}{4\delta_{c1}} & \frac{k_{c2}}{k_{c1}} \end{bmatrix}}_{A_{c1}} e_{c1} + \frac{c_{c4}}{2\delta_{c1}} \|\tilde{\Omega}_o\| \sqrt{\|\tilde{R}_c\|_I} \\ & + \frac{k_{c2}}{k_{c1}} \|\tilde{\Omega}_o\| \|\tilde{\Omega}_c\| \end{aligned} \quad (77)$$

$A_{c1}$  is positive if  $\delta_{c1} > \frac{c_{c3}^2}{8k_{c2}c_{c2}}$ . Let us set  $\delta_{c1} > \max\{\frac{\bar{\lambda}_J c_{c1}}{4} \sqrt{\frac{k_{c1}}{\lambda_J}}, \frac{c_{c3}^2}{8k_{c2}c_{c2}}\}$  with  $\lambda_{A_{c1}}$  being the minimum eigenvalue of  $A_{c1}$ . Recalling (60) and (71), one shows

$$\begin{cases} \dot{\mathcal{E}} = \tilde{V}_c - \dot{\theta} \\ \dot{\mathcal{E}} = F - \|ge_3 - F\|(R^\top - R_d^\top)e_3 - \ddot{P}_d - \ddot{\theta} \end{cases} \quad (78)$$

In view of (62) and (63), it becomes apparent that  $\ddot{\theta}$  and  $F$  are bounded indicating that  $\mathfrak{S}$  is bounded. Also, note that  $\|\mathbf{I}_3 - \tilde{R}_c\|_F = 2\sqrt{2}\sqrt{\|\tilde{R}_c\|_I}$  such that  $\|ge_3 - F\|(R^\top - R_d^\top)e_3 = \|ge_3 - F\|(\mathbf{I}_3 - \tilde{R}_c)R^\top e_3 \leq 4(\|ge_3\| + \sup_{t \geq 0}\{\|\ddot{P}_d\|\}) + (k_{\theta 1} + k_{\theta 2})\sqrt{\|\tilde{R}_c\|_I} \triangleq 4\pi\sqrt{\|\tilde{R}_c\|_I}$

$$\|ge_3 - F\|(R^\top - R_d^\top)e_3 \leq 4\pi\sqrt{\|\tilde{R}_c\|_I} \quad (79)$$

where  $\pi$  is an upper bounded positive constant. From (60) and (78), define the following Lyapunov function candidate:

$$\mathcal{L}_{c2} = \frac{1}{2}\mathcal{E}^\top \mathcal{E} + \frac{1}{2k_{c1}}\dot{\mathcal{E}}^\top \dot{\mathcal{E}} + \frac{1}{\delta_{c2}}\mathcal{E}^\top \dot{\mathcal{E}} \quad (80)$$

such that

$$e_{c2}^\top \underbrace{\begin{bmatrix} \frac{1}{2} & -\frac{1}{2\delta_{c2}} \\ -\frac{1}{2\delta_{c2}} & \frac{1}{2k_{c3}} \end{bmatrix}}_{M_7} e_{c2} \leq \mathcal{L}_{c2} \leq e_{c2}^\top \underbrace{\begin{bmatrix} \frac{1}{2} & \frac{1}{2\delta_{c2}} \\ \frac{1}{2\delta_{c2}} & \frac{1}{2k_{c3}} \end{bmatrix}}_{M_8} e_{c2}$$

where  $e_{c2} = [\|\mathcal{E}\|, \|\dot{\mathcal{E}}\|]^\top$ .  $M_7$  and  $M_8$  are made positive by selecting  $\delta_{c2} > \sqrt{k_{c3}}$ . Using (78), (63), (62), and (79), one obtains

$$\begin{aligned} \dot{\mathcal{L}}_{c2} \leq & -e_{c2}^\top \underbrace{\begin{bmatrix} \frac{k_{c3}}{\delta_{c2}} & \frac{k_{c4}}{2\delta_{c2}} \\ \frac{k_{c4}}{2\delta_{c2}} & \frac{k_{c4}}{k_{c3}} - \frac{1}{\delta_{c2}} \end{bmatrix}}_{A_{c2}} e_{c2} + (\|\dot{\mathcal{E}}\| + \frac{k_{c3}}{\delta_{c2}}\|\mathcal{E}\|)\|\tilde{P}_o\| \\ & + (\frac{k_{c4}}{k_{c3}}\|\dot{\mathcal{E}}\| + \frac{k_{c4}}{\delta_{c2}}\|\mathcal{E}\|)\|\tilde{V}_o\| + 4\pi(\|\dot{\mathcal{E}}\| + \frac{1}{\delta_{c2}}\|\mathcal{E}\|)\sqrt{\|\tilde{R}_c\|_I} \end{aligned} \quad (81)$$

Note that  $\hat{P} - P_d - \theta = -\tilde{P}_o + \mathcal{E}$  and  $\hat{V} - V_d - \dot{\theta} = -\tilde{V}_o + \dot{\mathcal{E}}$ .  $A_{c2}$  is made positive by selecting  $\delta_{c2} > \frac{k_{c4}^2 + 4k_{c3}}{4k_{c4}}$ . Consider selecting  $\delta_{c2} > \max\{\sqrt{k_{c3}}, \frac{k_{c4}^2 + 4k_{c3}}{4k_{c4}}\}$ . Based on (48),  $\tilde{P}_o$  and  $\tilde{V}_o$  are bounded and converge to zero, while from (73),  $\sqrt{\|\tilde{R}_c\|_I}$  is bounded. Therefore,  $\mathcal{L}_{c2}$  is bounded. Recall (80),

(76), and define the following Lyapunov function candidate  $\mathcal{L}_T : \mathbb{S}\mathbb{O}(3) \times \mathbb{R}^3 \times \mathbb{R}^3 \times \mathbb{R}^3 \rightarrow \mathbb{R}_+$ :

$$\mathcal{L}_{cT} = \mathcal{L}_{c1} + \mathcal{L}_{c2} \quad (82)$$

From (81) and (77), one obtains

$$\begin{aligned} \dot{\mathcal{L}}_{cT} \leq & -e_{c3}^\top \underbrace{\begin{bmatrix} \lambda_{A_{c1}} & -c_e \\ -c_e & \lambda_{A_{c2}} \end{bmatrix}}_{A_c} e_{c3} + (\|\dot{\mathcal{E}}\| + \frac{k_{c3}}{\delta_{c2}}\|\mathcal{E}\|)\|\tilde{P}_o\| \\ & + (\frac{k_{c2}}{k_{c1}}\|\tilde{\Omega}_c\| + \frac{c_{c4}}{2\delta_{c1}}\sqrt{\|\tilde{R}_c\|_I})\|\tilde{\Omega}_o\| \\ & + (\frac{k_{c4}}{k_{c3}}\|\dot{\mathcal{E}}\| + \frac{k_{c4}}{\delta_{c2}}\|\mathcal{E}\|)\|\tilde{V}_o\| \end{aligned} \quad (83)$$

where  $c_e = \max\{2\pi, \frac{2\pi}{\delta_{c2}}\}$  and  $e_{c3} = [\|e_{c1}\|, \|e_{c2}\|]^\top$ . For a positive definite  $A_c$ , select  $\lambda_{A_{c1}} > c_e^2/\lambda_{A_{c2}}$ . Let  $\lambda_{A_c}$  denote the minimum eigenvalue of  $A_c$ . Using (47) and (82), define the following Lyapunov function candidate:

$$\mathcal{L}_T = \mathcal{L}_{oT} + \mathcal{L}_{cT} \quad (84)$$

Thus, from (48) and (83), one finds

$$\begin{aligned} \dot{\mathcal{L}}_T \leq & -\lambda_{A_o}\|\tilde{R}_o\|_I - e_1^\top \underbrace{\begin{bmatrix} \lambda_{A_o} & \frac{c_{c4}}{4\delta_{c1}} & \frac{k_{c2}}{2k_{c1}} \\ \frac{c_{c4}}{4\delta_{c1}} & \lambda_{A_c} & 0 \\ \frac{k_{c2}}{2k_{c1}} & 0 & \lambda_{A_c} \end{bmatrix}}_{A_1} e_1 \\ & - e_2^\top \underbrace{\begin{bmatrix} \lambda_{A_o} \mathbf{I}_2 & \frac{c_p}{2} \mathbf{I}_2 \\ \frac{c_p}{2} \mathbf{I}_2 & \lambda_{A_c} \mathbf{I}_2 \end{bmatrix}}_{A_2} e_2 \end{aligned} \quad (85)$$

where  $e_1 = [\|\tilde{\Omega}_o\|, \sqrt{\|\tilde{R}_c\|_I}, \|\tilde{\Omega}_c\|]^\top$ ,  $e_2 = [\|\tilde{P}_o\|, \|\tilde{V}_o\|, \|\mathcal{E}\|, \|\dot{\mathcal{E}}\|]^\top$ , and  $c_p = \max\{1, \frac{k_{c3}}{\delta_{c2}}, \frac{k_{c4}}{k_{c3}}, \frac{k_{c4}}{\delta_{c2}}\}$ .  $A_1$  is positive if  $\lambda_{A_o} > \frac{4\delta_{c1}^2 k_{c2}^2 + k_{c1}^2 c_{c4}^2}{16\lambda_{A_c} k_{c1}^2 \delta_{c1}^2}$ , and  $A_2$  is positive if  $\lambda_{A_o} > \frac{c_p^2}{4\lambda_{A_c}}$ . Thus, consider selecting  $\lambda_{A_o} > \max\{\frac{c_p^2}{4\lambda_{A_c}}, \frac{4\delta_{c1}^2 k_{c2}^2 + k_{c1}^2 c_{c4}^2}{16\lambda_{A_c} k_{c1}^2 \delta_{c1}^2}\}$ . Let  $\lambda_{A_1}$  and  $\lambda_{A_2}$  denote the minimum eigenvalue of  $A_1$  and  $A_2$ , respectively. By defining  $\lambda_A = \min\{\lambda_{A_1}, \lambda_{A_2}, \lambda_{A_o}\}$  and  $\bar{\lambda}_M = \max\{\bar{\lambda}(M_1), \bar{\lambda}(M_2), \dots, \bar{\lambda}(M_8)\}$ , one finds

$$\begin{aligned} \dot{\mathcal{L}}_T & \leq -(\lambda_A/\bar{\lambda}_M)\mathcal{L}_T \\ \mathcal{L}_T(t) & \leq \mathcal{L}_T(0) \exp(-t\lambda_A/\bar{\lambda}_M), \quad \forall t \geq 0 \end{aligned} \quad (86)$$

such that  $\lim_{t \rightarrow \infty} \tilde{R}_o = \lim_{t \rightarrow \infty} \tilde{R}_c = \mathbf{I}_3$ ,  $\lim_{t \rightarrow \infty} \|\tilde{\Omega}_o\| = \lim_{t \rightarrow \infty} \|\tilde{P}_o\| = \lim_{t \rightarrow \infty} \|\tilde{V}_o\| = 0$ , and  $\lim_{t \rightarrow \infty} \|\tilde{\Omega}_c\| = \lim_{t \rightarrow \infty} \|\mathcal{E}\| = \lim_{t \rightarrow \infty} \|\dot{\mathcal{E}}\| = 0$ . From (86), the definition of  $\theta$  in (62) implies that  $\theta \rightarrow -k_{\theta 1}\psi(\theta) - k_{\theta 2}\psi(\dot{\theta})$  as  $\mathcal{E}, \dot{\mathcal{E}} \rightarrow 0$  and, in turn,  $\|\psi(\theta)\|$  and  $\|\psi(\dot{\theta})\|$  become strictly decreasing with  $\psi(\theta), \psi(\dot{\theta}) \rightarrow 0$  which shows that  $\lim_{t \rightarrow \infty} \theta = \lim_{t \rightarrow \infty} \dot{\theta} = 0$ . Therefore,  $\lim_{t \rightarrow \infty} \tilde{R}_o = \lim_{t \rightarrow \infty} \tilde{R}_c = \mathbf{I}_3$ ,  $\lim_{t \rightarrow \infty} \|\tilde{\Omega}_o\| = \lim_{t \rightarrow \infty} \|\tilde{P}_o\| = \lim_{t \rightarrow \infty} \|\tilde{V}_o\| = 0$ ,  $\lim_{t \rightarrow \infty} \|\tilde{\Omega}_c\| = \lim_{t \rightarrow \infty} \|\tilde{P}_c\| = \lim_{t \rightarrow \infty} \|\tilde{V}_c\| = 0$ , and the closed loop error signals of the observer-based controller design are uniformly almost globally exponentially stable proving Theorem 2. ■

## VI. IMPLEMENTATION STEPS

The VTOL-UAV observer-based controller on the Lie Group is presented in a discrete form to facilitate the implementation process. Define  $\Delta t$  as a small sample time step. The implementation steps are as follows:

**Step 1.** Select  $\hat{\Omega}_1, \hat{P}_0, \hat{V}_0, \theta_0, \dot{\theta}_0 \in \mathbb{R}^3, \hat{R}_0 \in \mathbb{SO}(3)$ , formulate the navigation matrix  $\hat{X}_0 = \begin{bmatrix} \hat{R}_0^\top & \hat{P}_0 & \hat{V}_0 \\ 0_{1 \times 3} & 1 & 0 \\ 0_{1 \times 3} & 0 & 1 \end{bmatrix}$ , and define  $k = 1$ .

**Step 2.** (Pose reconstruction) Use one of the methods of pose reconstruction to obtain reconstructed attitude  $R_{y|k}$  and position  $P_{y|k}$ . For more details consult [7], [8].

**Step 3.** (Pose estimation error) Evaluate the attitude error as  $\tilde{R}_{o|k} = R_y \hat{R}_{o|k}^\top$  and the position error as  $\tilde{P}_{o|k} = P_{y|k} - \hat{P}_{o|k}$ .

**Step 4.** (Thrust) Obtain  $F_k$  and  $\mathfrak{S}_k$  as in (63) and (64)

$$F_k = \ddot{P}_d - k_{\theta 1} \psi(\theta_{k-1}) - k_{\theta 2} \psi(\dot{\theta}_{k-1}) = [f_1, f_2, f_3]^\top$$

$$\mathfrak{S}_k = m \|g e_3 - F_k\|$$

with  $\ddot{\theta}_k = -k_{\theta 1} \psi(\theta_{k-1}) - k_{\theta 2} \psi(\dot{\theta}_{k-1}) + k_{c 3} (\hat{P}_{k-1} - P_{d|k} - \theta_{k-1}) + k_{c 4} (\hat{V}_{k-1} - V_{d|k} - \dot{\theta}_{k-1})$ ,  $\dot{\theta}_k = \dot{\theta}_{k-1} + \Delta t \ddot{\theta}_k$ , and  $\theta_k = \theta_{k-1} + \Delta t \dot{\theta}_k$ .

**Step 5.** (Prediction)  $\hat{U}_k = \begin{bmatrix} [\hat{\Omega}_{k-1}]_\times & 0_{3 \times 1} & -\frac{\mathfrak{S}_k}{m} e_3 \\ 0_{1 \times 3} & 0 & 0 \\ 0_{1 \times 3} & 1 & 0 \end{bmatrix}$

where  $\hat{U}_k \in \mathcal{U}_{\mathcal{M}}$  and

$$\hat{X}_{k|k-1} = \hat{X}_{k-1} \exp(\hat{U}_k \Delta t)$$

$\exp(\cdot)$  denotes exponential of a matrix.

**Step 6.** (Correction factors) Evaluate the correction factors as  $w_o = -\gamma_o \tilde{R}_{o|k}^\top \mathbf{vex}(\mathcal{P}_a(\tilde{R}_{o|k}))$ ,  $w_\Omega = k_{o 1} R_{y|k}^\top \mathbf{vex}(\mathcal{P}_a(\tilde{R}_{o|k}))$ ,  $w_V = -[w_\Omega]_\times \hat{P}_{k-1} - k_{o 2} \tilde{P}_{o|k}$ , and  $w_a = -\frac{\mathfrak{S}_k}{m} \hat{R}_{o|k}^\top (\mathbf{I}_3 - \tilde{R}_{o|k}^\top) e_3 - g e_3 - [w_\Omega]_\times \hat{V}_{k-1} - k_{o 3} \tilde{P}_{o|k}$

**Step 7.** (Correction)  $W = \begin{bmatrix} [w_\Omega]_\times & w_V & w_a \\ 0_{1 \times 3} & 0 & 0 \\ 0_{1 \times 3} & 1 & 0 \end{bmatrix} \in \mathcal{U}_{\mathcal{M}}$  and

$$\hat{X}_k = \exp(-W \Delta t) \hat{X}_{k|k-1}$$

where  $\hat{P}_k = \hat{X}_k(1 : 3, 4)$ ,  $\hat{V}_k = \hat{X}_k(1 : 3, 5)$ , and  $\hat{R}_k = \hat{X}_k(1 : 3, 1 : 3)^\top$ .

**Step 8.** Follow the Appendix to evaluate the derivatives of the intermediary control inputs  $\dot{F}_k$  and  $\dot{\tilde{F}}_k$ . Also,  $\Xi(F_k)$  is evaluated as in (58) along with its derivative  $\dot{\Xi}(F)$ .

**Step 9.** (Desired attitude) The desired unit-quaternion is

$$q_{d0|k} = \sqrt{\frac{m}{2\mathfrak{S}_k} (g - f_3) + \frac{1}{2}}, \quad q_{d|k} = \begin{bmatrix} \frac{m}{2\mathfrak{S}_k q_{d0}} f_2 \\ -\frac{m}{2\mathfrak{S}_k q_{d0}} f_1 \\ 0 \end{bmatrix}$$

where  $R_{d|k} = (q_{d0|k}^2 - \|q_{d|k}\|^2) \mathbf{I}_3 + 2q_{d|k} q_{d|k}^\top - 2q_{d0|k} [q_{d|k}]_\times \in \mathbb{SO}(3)$ .

**Step 10.** (Desired angular velocity) Calculate  $\Omega_{d|k} = \Xi(F_k) \dot{F}_k$  and  $\dot{\Omega}_{d|k} = \dot{\Xi}(F_k) \dot{F}_k + \Xi(F_k) \ddot{F}_k$  as in (57) and (59), respectively.

**Step 11.** (Rotational torque) Attitude error is evaluated by  $\tilde{R}_{c|k} = \hat{R}_k R_{d|k}^\top$  and the rotational torque is calculated as

$$\mathcal{T}_k = k_{c 1} \mathbf{vex}(\mathcal{P}_a(\tilde{R}_{c|k})) - k_{c 2} (\tilde{R}_{o|k} \hat{\Omega}_k - \tilde{R}_{c|k} \Omega_{d|k}) + \left[ \tilde{R}_{c|k} \Omega_{d|k} \right]_\times J \tilde{R}_{c|k} \Omega_{d|k} + J \tilde{R}_{c|k} \dot{\Omega}_{d|k}$$

**Step 12.** (Angular velocity estimate) The angular velocity estimate is evaluated by

$$\hat{\Omega}_{k+1} = \hat{\Omega}_k + \Delta t \hat{J}^{-1} ([\hat{J} \hat{\Omega}_k]_\times \hat{\Omega}_k + \hat{\mathcal{T}}_k - \hat{J} [\hat{\Omega}_k]_\times \hat{R}_k w_\Omega + w_o)$$

where  $\hat{\mathcal{T}}_k = \tilde{R}_{o|k}^\top \mathcal{T}_k$  and  $\hat{J} = \tilde{R}_{o|k}^\top J \tilde{R}_{o|k}$ .

**Step 13.** Set  $k = k + 1$ , and go to **Step 2**.

## VII. SIMULATION AND EXPERIMENTAL RESULTS

### A. Simulation Results

This subsection presents the output performance of the proposed observer-based controller for a 6 DoF VTOL-UAV. The observing and tracking control capabilities are tested in a discrete form at a low sampling rate of 1000 Hz against unknown random noise and constant bias corrupting the measurements. Consider the mass and the inertia matrix of the VTOL-UAV to be  $m = 2.5$  kg and  $J = \text{diag}(0.14, 0.2, 0.12)$  kg.m<sup>2</sup>, respectively. Let the desired trajectory be

$$P_d = 6 \begin{bmatrix} \sin(0.2t) \\ \sin(0.2t) \cos(0.2t) \\ \frac{1}{6}(4 + 0.15t) \end{bmatrix} \text{ m}$$

The total time is set to 50 seconds. Let the true initial orientation, angular velocity, position, and linear velocity of the VTOL-UAV be

$$R_0 = \begin{bmatrix} -0.2712 & -0.7130 & 0.6466 \\ 0.8655 & -0.4746 & -0.1603 \\ 0.4212 & 0.5162 & 0.7458 \end{bmatrix}$$

$$\Omega_0 = [0, 0, 0]^\top \text{ rad/sec}$$

$$P_0 = [-2, -1, 0]^\top \text{ m}$$

$$V_0 = [0, 0, 0]^\top \text{ m/sec}$$

Let the estimated initial orientation, angular velocity, position, and linear velocity of the vehicle be

$$\hat{R}_0 = \mathbf{I}_3$$

$$\hat{\Omega}_0 = \hat{P}_0 = \hat{V}_0 = [0, 0, 0]^\top$$

Let  $\hat{\theta}_0 = \dot{\hat{\theta}}_0 = [0, 0, 0]^\top$ . From (15),  $y_i^{\mathcal{B}} = R v_i^{\mathcal{I}} + b_i^{\mathcal{B}} + n_i^{\mathcal{B}}$  for  $i = 1, 2$ , let

$$\begin{cases} v_1^{\mathcal{I}} &= [0, 0, 1]^\top \\ v_2^{\mathcal{I}} &= [1, -1, -1]^\top \end{cases}$$

with  $b_1^{\mathcal{B}} = [0, 0, -0.15]^\top$ ,  $b_2^{\mathcal{B}} = [0.1, 0.09, -0.11]^\top$ , and normally distributed noise  $n_1^{\mathcal{B}}$  and  $n_2^{\mathcal{B}}$  having a zero mean and a STD of 0.05, in other words  $\mathcal{N}(0, 0.05)$ . The attitude

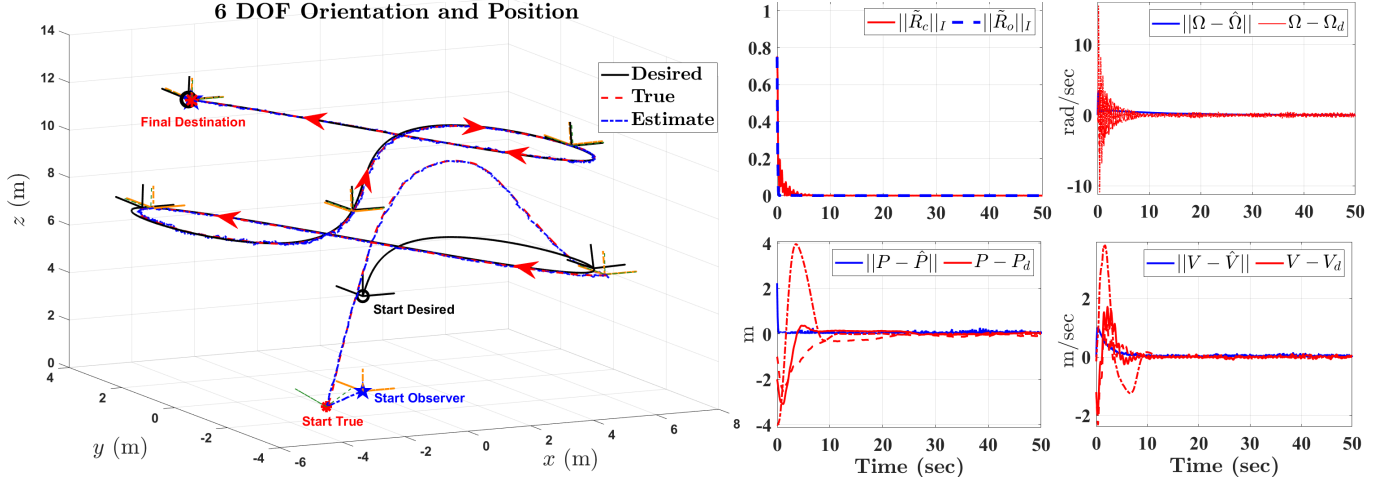


Fig. 3. Output performance of the observer-based controller implemented using a 6 DoF VTOL-UAV. The left portion illustrates the desired position (black solid line), the true position (red dashed line), and the estimated position (blue center line). The VTOL-UAV orientation (roll, yaw, and pitch) is shown as a black solid line, a green dashed line, and an orange center line corresponding to the desired, true, and estimated orientation, respectively. Convergence of the error trajectories is demonstrated in the right portion where blue and red denote the error components between the true and the observed data, and between the true and the desired data, respectively.

is reconstructed using SVD [1] where  $v_3^I = v_1^I \times v_2^I$  and  $y_3^B = y_1^B \times y_2^B$ :

$$\begin{cases} \mathbf{r}_i = \frac{v_i^I}{\|v_i^I\|}, & \mathbf{y}_i = \frac{y_i^B}{\|y_i^B\|}, & i = 1, 2, \dots, N \\ B = \sum_{i=1}^n s_i \mathbf{y}_i \mathbf{r}_i^T = U S V^T \\ U_+ = U \cdot \text{diag}(1, 1, \det(U)) \\ V_+ = V \cdot \text{diag}(1, 1, \det(V)) \\ R_y = V_+ U_+^T \end{cases} \quad (87)$$

Consider a group of seven non-collinear randomly distributed landmarks ( $N_2 = 7$ ) satisfying Assumption 1 item A1. Let  $s_j = 1 \forall j = 1, 2, \dots, 7$  and  $s_c = \sum_{j=1}^{N_2} s_j$ . The landmark measurements are defined as in (16) and incorporate added constant bias and normally distributed noise ( $\mathcal{N}(0, 0.05)$ ). The position at each time instant is reconstructed as (see (17)):

$$\begin{cases} p_c = \frac{1}{s_c} \sum_{j=1}^{N_2} s_j p_j^T, & z_c = \frac{1}{s_c} \sum_{j=1}^{N_2} s_j z_j^B \\ P_y = p_c - R_y^T z_c \end{cases} \quad (88)$$

For more details of attitude and pose reconstruction visit [7], [8]. Let the design parameters be selected as follows:  $\gamma_o = 0.1$ ,  $k_{o1} = 10$ ,  $k_{o2} = 10$ ,  $k_{o3} = 5$ ,  $k_{c1} = 10$ ,  $k_{c2} = 0.1$ ,  $k_{c1} = 2$ ,  $k_{c2} = 4$ ,  $k_{\theta1} = 1$ , and  $k_{\theta2} = 1$ .

Fig. 3 demonstrates the output performance of a VTOL-UAV guided by the observer-based controller. Fig. 3 shows robust, strong, fast, and smooth tracking performance of the proposed observer-based controller and its ability to guide the VTOL-UAV to the desired final destination, despite a large initial error. The error is shown to rapidly converge from large initial values to the neighborhood of the attractive equilibrium point. Fig. 4 depicts the bounded rotational torque input and the thrust input.

### B. Experimental Results

To further validate the observing capabilities, the proposed observer with the appropriate modification has been tested

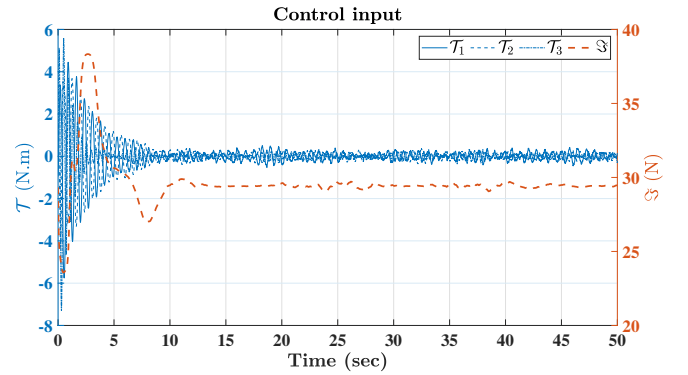


Fig. 4. VTOL-UAV control input.

using the EuRoC real-world dataset [35] that includes the ground truth of a real-life quadrotor flight trajectory, stereo images, and IMU data. The ADIS16448 IMU collected data at a sampling rate of 200 Hz. The MT9V034 sensor collected stereo images at a sampling rate of 20 Hz which were subsequently undistorted with the camera parameters and calibrated using a Stereo Camera Calibrator in MATLAB. For more details about the EuRoC dataset visit [35]. The landmarks were tracked using minimum eigenvalue landmark detection through Kanade-Lucas-Tomasi (KLT) feature tracker [36], see Fig. 5. Due to the fact that the dataset had no landmark information, a set of landmarks was generated from the stereo images using  $p_j^T = R^T z_j^B + P$  where  $P$  and  $R$  denote ground truth position and orientation, respectively. For the purposes of the experiment, the maximum number of detected landmarks was limited to 50. The coordinates of the landmark camera frame (cam0 EuRoC dataset) were transformed to the vehicle frame using the calibration matrix included in the dataset.

The experimental results shown in Fig. 6 reveal strong tracking capability of the proposed observer demonstrating the

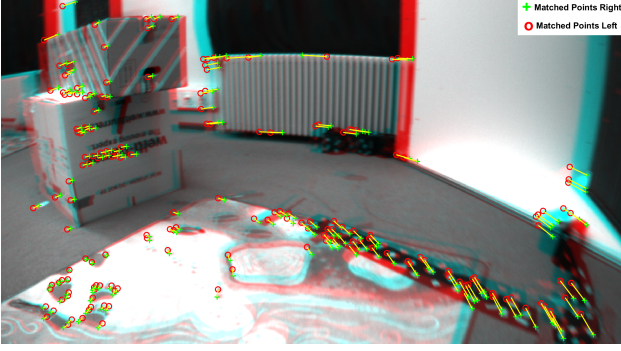


Fig. 5. An example of landmark detection and tracking. Photographs are obtained from the EuRoC dataset [35].

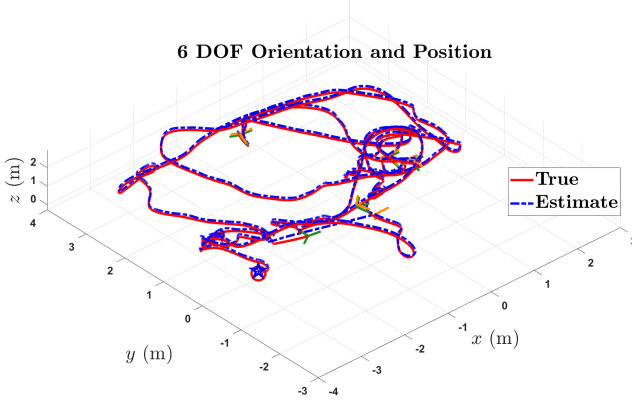


Fig. 6. Experimental validation using the Vicon Room 2 02 dataset. Output performance of the proposed observer for a 6 DoF UAV.

robustness of the proposed approach. To summarize, Fig. 3 and 6 illustrate the effectiveness of the proposed observer-based controller to observe the unknown motion parameters, namely orientation, angular velocity, position, and linear velocity, while tracking the vehicle along the desired trajectory.

## VIII. CONCLUSION

This paper addressed the estimation and control of the motion parameters, namely attitude, angular velocity, position, and linear velocity, in application to a six degrees of freedom (6 DoF) Vertical Take-Off and Landing Unmanned Aerial Vehicle (VTOL-UAV). The newly proposed observer-based controller as well as the observer that lies at its foundation are both characterized by almost global exponential stability of the closed loop error signals regardless of the initial condition. The proposed approach does not require a gyroscope and Global Positioning Systems signals. Use of measurements obtained by a low-cost measurement unit at a low sampling rate do not compromise the performance of the proposed observer-based controller. On the contrary, as has been revealed by simulation and experimental results, the proposed approach is distinguished by accurate observation and robust tracking control to the desired trajectory of the VTOL-UAV motion parameters, namely attitude, angular velocity, position, and linear velocity.

## ACKNOWLEDGMENT

The authors would like to thank **Maria Shaposhnikova** for proofreading the article.

## Appendix A

Let  $\theta \in \mathbb{R}^3$  be an auxiliary variable defined in (60). Define the mapping of

$$\psi(\theta_i) = \frac{\exp(\theta_i) - \exp(-\theta_i)}{\exp(\theta_i) + \exp(-\theta_i)}, \quad \forall i = 1, 2, 3$$

and

$$\psi(\dot{\theta}_i) = \frac{\exp(\dot{\theta}_i) - \exp(-\dot{\theta}_i)}{\exp(\dot{\theta}_i) + \exp(-\dot{\theta}_i)}, \quad \forall i = 1, 2, 3$$

such that  $\psi(\theta) = [\psi(\theta_1), \psi(\theta_2), \psi(\theta_3)]^\top \in \mathbb{R}^3$  and  $\psi(\dot{\theta}) = [\psi(\dot{\theta}_1), \psi(\dot{\theta}_2), \psi(\dot{\theta}_3)]^\top \in \mathbb{R}^3$ . One can easily show that  $\frac{d}{dt}\psi(\theta_i) = (1 - \psi(\theta_i)^2)\dot{\theta}_i$ ,  $\frac{d^2}{dt^2}\psi(\theta_i) = (1 - \psi(\theta_i)^2)(\ddot{\theta}_i - 2\psi(\theta_i)\dot{\theta}_i^2)$ ,  $\frac{d}{dt}\psi(\dot{\theta}_i) = (1 - \psi(\dot{\theta}_i)^2)\ddot{\theta}_i$ , and  $\frac{d^2}{dt^2}\psi(\dot{\theta}_i) = (1 - \psi(\dot{\theta}_i)^2)(\theta_i^{(3)} - 2\psi(\dot{\theta}_i)\ddot{\theta}_i^2)$ . Therefore, the first and the second derivatives of  $F$  are as follows:

$$\begin{aligned} \dot{F} &= P_d^{(3)} - k_{\theta 1} \frac{d}{dt}\psi(\theta) - k_{\theta 2} \frac{d}{dt}\psi(\dot{\theta}) \\ \ddot{F} &= P_d^{(4)} - k_{\theta 1} \frac{d^2}{dt^2}\psi(\theta) - k_{\theta 2} \frac{d^2}{dt^2}\psi(\dot{\theta}) \end{aligned}$$

with

$$\begin{aligned} \theta^{(3)} &= -k_{\theta 1} \frac{d}{dt}\psi(\theta) - k_{\theta 2} \frac{d}{dt}\psi(\dot{\theta}) + k_{c1}(\dot{P} - \dot{P}_d - \dot{\theta}) \\ &\quad + k_{c2}(\dot{V} - \dot{V}_d - \ddot{\theta}) \end{aligned}$$

where  $P_d^{(3)} = \frac{d^3}{dt^3}P_d$ ,  $P_d^{(4)} = \frac{d^4}{dt^4}P_d$ , and  $\theta^{(3)} = \frac{d^3}{dt^3}\theta$ . In addition,  $\dot{\alpha}_1 = \frac{1}{\alpha_1}[f_1, f_2, (f_3 - g)]^\top \dot{F}$  and  $\dot{\alpha}_2 = \dot{\alpha}_1 - f_3$  with  $\dot{F} = [f_1, f_2, f_3]^\top$ .

## Appendix B

### Quaternion Representation of the Observer-based Controller

Recall Section II and let  $Q_y = [q_{y0}, q_y^\top]^\top \in \mathbb{S}^3$  be the reconstructed attitude, obtained for instance, using QUEST algorithm [37]. Define the reconstructed attitude  $\mathcal{R}_y : \mathbb{S}^3 \rightarrow \mathbb{SO}(3)$  as (see (9)):

$$\mathcal{R}_y = (q_{y0}^2 - \|q_y\|^2)\mathbf{I}_3 + 2q_y q_y^\top - 2q_{y0}[q_y]_\times \in \mathbb{SO}(3)$$

Define  $\hat{Q} = [\hat{q}_0, \hat{q}^\top]^\top \in \mathbb{S}^3$  as the estimate of  $Q = [q_0, q^\top]^\top \in \mathbb{S}^3$ . Define the estimated attitude  $\hat{\mathcal{R}} : \mathbb{S}^3 \rightarrow \mathbb{SO}(3)$  as

$$\hat{\mathcal{R}} = (\hat{q}_0^2 - \|\hat{q}\|^2)\mathbf{I}_3 + 2\hat{q}\hat{q}^\top - 2\hat{q}_0[\hat{q}]_\times \in \mathbb{SO}(3)$$

Let the error in estimation be  $\tilde{Q}_o = \hat{Q}^{-1} \odot Q_y = [\tilde{q}_{o0}, \tilde{q}_o^\top]^\top \in \mathbb{S}^3$ . Define the error between the estimated and the true attitude  $\tilde{\mathcal{R}}_o : \mathbb{S}^3 \rightarrow \mathbb{SO}(3)$  as

$$\tilde{\mathcal{R}}_o = (\tilde{q}_{o0}^2 - \|\tilde{q}_o\|^2)\mathbf{I}_3 + 2\tilde{q}_o \tilde{q}_o^\top - 2\tilde{q}_{o0}[\tilde{q}_o]_\times \in \mathbb{SO}(3)$$

Let the error in control be  $\tilde{Q}_c = Q_d^{-1} \odot \hat{Q} = [\tilde{q}_{c0}, \tilde{q}_c^\top]^\top \in \mathbb{S}^3$  and define the error between the desired and the true attitude  $\tilde{\mathcal{R}}_c : \mathbb{S}^3 \rightarrow \mathbb{SO}(3)$  as

$$\tilde{\mathcal{R}}_c = (\tilde{q}_{c0}^2 - \|\tilde{q}_c\|^2)\mathbf{I}_3 + 2\tilde{q}_c \tilde{q}_c^\top - 2\tilde{q}_{c0}[\tilde{q}_c]_\times \in \mathbb{SO}(3)$$

The quaternion representation of the observer in (24)-(29) is as below:

$$\begin{cases} \Phi &= \begin{bmatrix} 0 & -\hat{\Omega}^\top \\ \hat{\Omega} & -[\hat{\Omega}]_\times \end{bmatrix}, \quad \Psi = \begin{bmatrix} 0 & -w_\Omega^\top \\ w_\Omega & [w_\Omega]_\times \end{bmatrix} \\ \dot{Q} &= \frac{1}{2}(\Phi - \Psi)\dot{Q} \\ \dot{J}\hat{\Omega} &= [\hat{J}\hat{\Omega}]_\times \hat{\Omega} + \hat{T} - \hat{J}[\hat{\Omega}]_\times \hat{R}w_\Omega + w_o \\ \dot{\hat{P}} &= \hat{V} - [w_\Omega]_\times \hat{P} - w_V \\ \dot{\hat{V}} &= -\frac{\mathfrak{S}}{m}\hat{R}^\top e_3 - [w_\Omega]_\times \hat{V} - w_a \end{cases}$$

where  $\hat{T} = \tilde{R}_o^\top \mathcal{T}$ ,  $\hat{J} = \tilde{R}_o^\top J \tilde{R}_o$ , and

$$\begin{cases} w_o &= -2\gamma_o \tilde{q}_{o0} \tilde{R}_o^\top \tilde{q}_o \\ w_\Omega &= 2k_{o1} \tilde{q}_{o0} \tilde{R}_y^\top \tilde{q}_o \\ w_V &= -[w_\Omega]_\times \hat{P} - k_{o2} \tilde{P}_o, \quad \tilde{P}_o = P_y - \hat{P} \\ w_a &= -\frac{\mathfrak{S}}{m} \tilde{R}^\top (\mathbf{I}_3 - \tilde{R}_o^\top) e_3 - g e_3 - [w_\Omega]_\times \hat{V} - k_{o3} \tilde{P}_o \end{cases}$$

where  $\Upsilon(\tilde{R}_o) = 2\tilde{q}_{o0}\tilde{q}_o$  (see [31], [32]). The quaternion representation of the control laws in (61)-(64) is as below:

$$\begin{cases} \mathcal{T} &= 2k_{c1}\tilde{q}_{c0}\tilde{q}_c - k_{c2}(\tilde{R}_o\hat{\Omega} - \tilde{R}_c\Omega_d) + J\tilde{R}_c\hat{\Omega}_d \\ &\quad + [\tilde{R}_c\Omega_d]_\times J\tilde{R}_c\Omega_d \\ \dot{\theta} &= -k_{\theta 1}\psi(\theta) - k_{\theta 2}\psi(\dot{\theta}) + k_{c3}(\hat{P} - P_d - \theta) \\ &\quad + k_{c4}(\hat{V} - V_d - \dot{\theta}) \\ F &= \ddot{P}_d - k_{\theta 1}\psi(\theta) - k_{\theta 2}\psi(\dot{\theta}) \\ \mathfrak{S} &= m\|ge_3 - F\| \end{cases}$$

where  $\Upsilon(\tilde{R}_c) = 2\tilde{q}_{c0}\tilde{q}_c$ . To know more about attitude parameterization and mapping visit [32].

## REFERENCES

- [1] F. L. Markley, "Attitude determination using vector observations and the singular value decomposition," *Journal of the Astronautical Sciences*, vol. 36, no. 3, pp. 245–258, 1988.
- [2] D. Mortari, "Second estimator of the optimal quaternion," *Journal of Guidance, Control, and Dynamics*, vol. 23, no. 5, pp. 885–888, 2000.
- [3] F. L. Markley, "Attitude error representations for kalman filtering," *Journal of guidance, control, and dynamics*, vol. 26, no. 2, pp. 311–317, 2003.
- [4] L. Chang, F. Zha, and F. Qin, "Indirect kalman filtering based attitude estimation for low-cost attitude and heading reference systems," *IEEE/ASME Transactions on Mechatronics*, vol. 22, no. 4, pp. 1850–1858, 2017.
- [5] M. D. Pham, K. S. Low, S. T. Goh, and S. Chen, "Gain-scheduled extended kalman filter for nanosatellite attitude determination system," *IEEE Transactions on Aerospace and Electronic Systems*, vol. 51, no. 2, pp. 1017–1028, 2015.
- [6] D. E. Zlotnik and J. R. Forbes, "Exponential convergence of a nonlinear attitude estimator," *Automatica*, vol. 72, pp. 11–18, 2016.
- [7] H. A. Hashim, "Systematic convergence of nonlinear stochastic estimators on the special orthogonal group SO(3)," *International Journal of Robust and Nonlinear Control*, vol. 30, no. 10, pp. 3848–3870, 2020.
- [8] H. A. Hashim and F. L. Lewis, "Nonlinear stochastic estimators on the special euclidean group SE(3) using uncertain imu and vision measurements," *IEEE Transactions on Systems, Man, and Cybernetics: Systems*, vol. 51, no. 12, pp. 7587–7600, 2020.
- [9] A. Moeini and M. Namvar, "Global attitude/position estimation using landmark and biased velocity measurements," *IEEE Transactions on Aerospace and Electronic Systems*, vol. 52, no. 2, pp. 852–862, 2016.
- [10] H. A. Hashim, M. Abouheaf, and M. A. Abido, "Geometric stochastic filter with guaranteed performance for autonomous navigation based on imu and feature sensor fusion," *Control Engineering Practice*, vol. 116, p. 104926, 2021.
- [11] V. Pesce, S. Silvestrini, and M. Lavagna, "Radial basis function neural network aided adaptive extended kalman filter for spacecraft relative navigation," *Aerospace Science and Technology*, vol. 96, p. 105527, 2020.
- [12] R. Lozano, S. Salazar, D. Flores, and I. González-Hernández, "Pvtol global stabilisation using a nested saturation control," *International Journal of Control*, pp. 1–11, 2021.
- [13] H. Xie and A. F. Lynch, "State transformation-based dynamic visual servoing for an unmanned aerial vehicle," *International Journal of Control*, vol. 89, no. 5, pp. 892–908, 2016.
- [14] H. A. Hashim, "Guaranteed performance nonlinear observer for simultaneous localization and mapping," *IEEE Control Systems Letters*, vol. 5, no. 1, pp. 91–96, 2021.
- [15] D. Scaramuzza and et al., "Vision-controlled micro flying robots: from system design to autonomous navigation and mapping in gps-denied environments," *IEEE Robotics & Automation Magazine*, vol. 21, no. 3, pp. 26–40, 2014.
- [16] H. Qin, Z. Meng, W. Meng, X. Chen, H. Sun, F. Lin, and M. H. Ang, "Autonomous exploration and mapping system using heterogeneous uavs and ugvs in gps-denied environments," *IEEE Transactions on Vehicular Technology*, vol. 68, no. 2, pp. 1339–1350, 2019.
- [17] H. A. Hashim, "GPS-denied navigation: Attitude, position, linear velocity, and gravity estimation with nonlinear stochastic observer," in *2021 American Control Conference (ACC)*. IEEE, 2021, pp. 1149–1154.
- [18] F. Aghili and C.-Y. Su, "Robust relative navigation by integration of icp and adaptive kalman filter using laser scanner and imu," *IEEE/ASME Transactions on Mechatronics*, vol. 21, no. 4, pp. 2015–2026, 2016.
- [19] A. Barrau and S. Bonnabel, "The invariant extended kalman filter as a stable observer," *IEEE Transactions on Automatic Control*, vol. 62, no. 4, pp. 1797–1812, 2016.
- [20] "Nasa's hubble space telescope returns to science operations," *NASA TV*, 2018. [Online]. Available: <https://www.nasa.gov/hubble>
- [21] A. Roza and M. Maggiore, "A class of position controllers for underactuated vtol vehicles," *IEEE Transactions on Automatic Control*, vol. 59, no. 9, pp. 2580–2585, 2014.
- [22] S. Su and Y. Lin, "Robust output tracking control of a class of non-minimum phase systems and application to vtol aircraft," *International Journal of Control*, vol. 84, no. 11, pp. 1858–1872, 2011.
- [23] H. Rios, R. Falcon, O. A. Gonzalez, and A. Dzul, "Continuous sliding-mode control strategies for quadrotor robust tracking: real-time application," *IEEE Transactions on Industrial Electronics*, vol. 66, no. 2, pp. 1264–1272, 2018.
- [24] L. Besnard, Y. B. Shtessel, and B. Landrum, "Quadrotor vehicle control via sliding mode controller driven by sliding mode disturbance observer," *Journal of the Franklin Institute*, vol. 349, no. 2, pp. 658–684, 2012.
- [25] A. Drouot, E. Richard, and M. Boutayeb, "Hierarchical backstepping-based control of a gun launched mav in crosswinds: Theory and experiment," *Control Engineering Practice*, vol. 25, pp. 16–25, 2014.
- [26] M.-D. Hua, T. Hamel, P. Morin, and C. Samson, "A control approach for thrust-propelled underactuated vehicles and its application to vtol drones," *IEEE Transactions on Automatic Control*, vol. 54, no. 8, pp. 1837–1853, 2009.
- [27] D. Zheng, H. Wang, J. Wang, S. Chen, W. Chen, and X. Liang, "Image-based visual servoing of a quadrotor using virtual camera approach," *IEEE/ASME Transactions on Mechatronics*, vol. 22, no. 2, pp. 972–982, 2016.
- [28] J. Chen, C. Hua, and X. Guan, "Image based fixed time visual servoing control for the quadrotor uav," *IET Control Theory & Applications*, vol. 13, no. 18, pp. 3117–3123, 2019.
- [29] A. Mokhtari, N. K. M'Sirdi, K. Meghriche, and A. Belaidi, "Feedback linearization and linear observer for a quadrotor unmanned aerial vehicle," *Advanced Robotics*, vol. 20, no. 1, pp. 71–91, 2006.
- [30] D. Lee, T. Ryan, and H. J. Kim, "Autonomous landing of a vtol uav on a moving platform using image-based visual servoing," in *2012 IEEE international conference on robotics and automation*. IEEE, 2012, pp. 971–976.
- [31] M. D. Shuster, "A survey of attitude representations," *Navigation*, vol. 8, no. 9, pp. 439–517, 1993.
- [32] H. A. Hashim, "Special orthogonal group SO(3), euler angles, angle-axis, rodriguez vector and unit-quaternion: Overview, mapping and challenges," *arXiv preprint arXiv:1909.06669*, 2019.
- [33] A. Roberts and A. Tayebi, "Adaptive position tracking of vtol- uavs," in *Proceedings of the 48th IEEE conference on Decision and Control (CDC)*. IEEE, 2009, pp. 5233–5238.
- [34] A. Abdessameud and A. Tayebi, "Position tracking for vtol uavs," in *Motion Coordination for VTOL Unmanned Aerial Vehicles*. Springer, 2013, pp. 85–104.

- [35] M. Burri, J. Nikolic, P. Gohl, T. Schneider, J. Rehder, S. Omari, M. W. Achtelik, and R. Siegwart, "The euroc micro aerial vehicle datasets," *The International Journal of Robotics Research*, vol. 35, no. 10, pp. 1157–1163, 2016.
- [36] J. Shi *et al.*, "Good features to track," in *1994 Proceedings of IEEE conference on computer vision and pattern recognition*. IEEE, 1994, pp. 593–600.
- [37] M. D. Shuster and S. D. Oh, "Three-axis attitude determination from vector observations," *Journal of Guidance, Control, and Dynamics*, vol. 4, pp. 70–77, 1981.